Chemistry and Physics of Lipids 169 (2013) 27–38

Contents lists available at SciVerse ScienceDirect

Chemistry and Physics of Lipids

journal homepage: www.elsevier.com/locate/chemphyslip

The cost of living in the membrane: A case study of hydrophobic mismatch for the multi-segment protein LeuT

Sayan Mondal[a], George Khelashvili[a], Lei Shi[a,b], Harel Weinstein[a,b,*]

[a] Department of Physiology and Biophysics, Weill Cornell Medical College, Cornell University, New York, NY 10065, United States
[b] The HRH Prince Alwaleed Bin Talal Bin Abdulaziz Alsaud Institute for Computational Biomedicine, Weill Cornell Medical College, Cornell University, New York, NY 10065, United States

ARTICLE INFO

Article history:
Available online 30 January 2013

Keywords:
Lipid–protein interactions
Hydrophobic mismatch
Residual exposure energy
Leucine transporter
Neurotransmitter:sodium symporters
Multi-segment transmembrane proteins
Molecular dynamics simulations
Membrane deformation energy

ABSTRACT

Many observations of the role of the membrane in the function and organization of transmembrane (TM) proteins have been explained in terms of hydrophobic mismatch between the membrane and the inserted protein. For a quantitative investigation of this mechanism in the lipid–protein interactions of functionally relevant conformations adopted by a multi-TM segment protein, the bacterial leucine transporter (LeuT), we employed a novel method, Continuum-Molecular Dynamics (CTMD), that quantifies the energetics of hydrophobic mismatch by combining the elastic continuum theory of membrane deformations with an atomistic level description of the radially asymmetric membrane–protein interface from MD simulations. LeuT has been serving as a model for structure–function studies of the mammalian neurotransmitter:sodium symporters (NSSs), such as the dopamine and serotonin transporters, which are the subject of intense research in the field of neurotransmission. The membrane models in which LeuT was embedded for these studies were composed of 1-palmitoyl-2-oleoyl-sn-glycero-3-phosphocholine (POPC) lipid, or 3:1 mixture of 1-palmitoyl-2-oleoyl-sn-glycero-3-phosphoethanolamine (POPE) and 1-palmitoyl-2-oleoyl-sn-glycero-3-phosphoglycerol (POPG) lipids. The results show that deformation of the host membrane alone is not sufficient to alleviate the hydrophobic mismatch at specific residues of LeuT. The calculations reveal significant membrane thinning and water penetration due to the specific local polar environment produced by the charged K288 of TM7 in LeuT, that is membrane-facing deep inside the hydrophobic milieu of the membrane. This significant perturbation is shown to result in unfavorable polar–hydrophobic interactions at neighboring hydrophobic residues in TM1a and TM7. We show that all the effects attributed to the K288 residue (membrane thinning, water penetration, and the unfavorable polar–hydrophobic interactions at TM1a and TM7), are abolished in calculations with the K288A mutant. The involvement of hydrophobic mismatch is somewhat different in the functionally distinct conformations (outward-open, occluded, inward-open) of LeuT, and the differences are shown to connect to structural elements (e.g., TM1a) known to play key roles in transport. This finding suggests a mechanistic hypothesis for the enhanced transport activity observed for the K288A mutant, suggesting that the unfavorable hydrophobic–hydrophilic interactions hinder the motion of TM1a in the functionally relevant conformational transition to the inward-open state. Various extents of such unfavorable interactions, involving exposure to the lipid environment of adjacent hydrophobic and polar residues, are common in multi-segment transmembrane proteins, and must be considered to affect functionally relevant conformational transitions.

1. Introduction

The membrane environment has been shown to play a significant role in the function and organization of various membrane proteins such as GPCRs and ion channels. Documented examples include the oligomerization and activation of rhodopsin, a prototypical GPCR (Botelho et al., 2002, 2006; Brown, 1994; Brown et al., 2002; Soubias et al., 2010), the inactivation of voltage-dependent sodium channels (Lundbaek et al., 2005; Rusinova et al., 2011), and the gating of mechanosensitive ion channels (Perozo et al., 2002; Phillips et al., 2009). Many such observations have been explained in terms of the energy cost due to the hydrophobic mismatch between the membrane and the protein (Andersen and Koeppe, 2007; Goforth et al., 2003; Huang, 1986; Nielsen et al., 1998; Phillips et al., 2009; Soubias et al., 2010).

* Corresponding author at: Department of Physiology and Biophysics, Weill Cornell Medical College, Cornell University, United States. Tel.: +1 212 746 6358; fax: +1 212 746 8690.
E-mail address: haw2002@med.cornell.edu (H. Weinstein).

0009-3084/$ – see front matter © 2013 Elsevier Ireland Ltd. All rights reserved.
http://dx.doi.org/10.1016/j.chemphyslip.2013.01.006

In response to the hydrophobic mismatch between the protein and the membrane in which it is inserted, the membrane deforms with a tendency to alleviate the mismatch (Harroun et al., 1999a). However, the hydrophobic matching by membrane deformation alone may remain incomplete (Marsh, 2008; Soubias et al., 2008), especially if the inserted protein is composed of several transmembrane (TM) segments that have different hydrophobic thicknesses (Mondal et al., 2011). The multi-segment TM proteins present to the surrounding membrane a radially asymmetric hydrophobic surface that imposes spatial constraints as a result of the energetic drive to match different hydrophobic lengths coming together in localized neighborhoods (Mondal et al., 2011). Consequently, the membrane deformation may not alleviate fully the hydrophobic mismatch. Indeed, our recent computational investigation of membrane–protein interactions of 7-TM segment GPCRs revealed that (i) the local membrane deformation profile is radially asymmetric, in response to the radially asymmetric hydrophobic surface of these 7-TM membrane proteins; (ii) notwithstanding local membrane deformations, the hydrophobic mismatch was not able to alleviate completely the exposure of specific residues to unfavorable polar–hydrophobic interactions (residual exposure); (iii) the energy penalty associated with the residual exposure (the residual exposure energy) is likely to have a spatially organizing role in the oligomerization properties of the GPCRs (Mondal et al., 2011, 2012); and (iv) membrane–protein interactions of very similar proteins can be very different due to the effect of just a few key differences in sequence (Mondal et al., 2012). Furthermore, we found that the binding of different ligands to the same GPCR can induce different conformations characterized by the orientation of specific TMs and loops, which produce distinct interactions of the membrane (Shan et al., 2012).

These findings were made possible by application of a novel approach to the computational models of the systems equilibrated with extensive molecular dynamics (MD) simulations, the Continuum-Molecular Dynamics (CTMD) method. This method quantifies the energetics of hydrophobic mismatch, taking into account the radial asymmetry of the hydrophobic surface of multi-segment transmembrane proteins and its effect on the surrounding membrane. It achieves this by combining the well-known elastic continuum theory of membrane deformations with an atomistic level description of the asymmetric membrane–protein interface from the cognate MD simulations (Mondal et al., 2011).

As demonstrated recently for GPCRs (Shan et al., 2012), our new CTMD approach can reveal distinct membrane–protein interactions associated with the different conformations adopted by multi-TM segment proteins in their functional mechanisms. This motivated our ongoing studies of the involvement of protein–membrane interaction in the function of another important family of multi-segment integral proteins – the neurotransmitter:sodium symporters (NSSs, TC code 2.A.22 (Saier, 1999)). From a series of multi-disciplinary studies of several members of this family of membrane proteins in a structural and mechanistic context, we have identified function-related conformational rearrangements and dynamic properties of the bacterial leucine transporter, LeuT (Shi et al., 2008; Zhao et al., 2010, 2011), for which a number of ligand-bound crystal structures are available (Krishnamurthy and Gouaux, 2012; Nyola et al., 2010; Piscitelli et al., 2010; Singh et al., 2008, 2007; Yamashita et al., 2005). Insights into various aspects of the structure and the functional mechanisms of LeuT were sought not only from the X-ray crystallography of LeuT in multiple conformations and in complex with different substrates or inhibitors (Krishnamurthy and Gouaux, 2012; Quick et al., 2009; Singh et al., 2008; Yamashita et al., 2005; Zhou et al., 2009), but also from dynamic measurements with EPR (Claxton et al., 2010) and single molecule FRET (Zhao et al., 2010, 2011), as well as from functional assays (Shi et al., 2008), and molecular dynamics simulations (Shaikh and Tajkhorshid, 2010; Shi et al., 2008; Zhao et al., 2010, 2011, 2012). These studies have identified key conformational changes of LeuT during substrate transport, the most notable change being the movement of the cytoplasmic segment of TM1 away from the TM-bundle during the transition of LeuT from outward-open to inward-open conformations (Krishnamurthy and Gouaux, 2012; Zhao et al., 2010, 2011).

The high degree of sequence homology of LeuT with the human neurotransmitter transporters (Beuming et al., 2006), and the high resolution crystal structures available for this protein have established LeuT as the prototypical model for studying the NSS family (Beuming et al., 2008, 2006). Moreover, it is now clear as well that many other transporters that do not exhibit an obvious sequence similarity to LeuT, such as the betaine transporter BetP and the proton-dependent transporter ApcT from the amino acid–polyamine–organocation family, share a common "LeuT-like" fold (Perez et al., 2011; Shaffer et al., 2009) and mechanism (Shi and Weinstein, 2010).

The information regarding structure–function relations for LeuT has guided our studies of the human NSS homologs, i.e., the transporters for dopamine (DAT) and serotonin (SERT) (Beuming et al., 2008, 2006; Shan et al., 2011). The physiological and medical significance of such an understanding stems from the important role the NSS transporters in neurotransmission. They are secondary active transporters that terminate neurotransmission by Na^+-driven uptake of the neurotransmitter from the synaptic cleft (Sonders et al., 2005). Not surprisingly, therefore, they are targeted by important medications such as the transporter-specific antidepressants (Zhou et al., 2009), but they are also the target of psychostimulant drugs of abuse like cocaine and amphetamine (Amara and Sonders, 1998). The thermodynamically uphill transport of substrate by the NSS transporters is driven by the co-transport of sodium down its electrochemical gradient, and the substrate transport involves major conformational changes of the transporter, generally considered to connect the outward-open to inward-open conformations in the spirit of a well-weathered alternating access theory (Jardetzky, 1966).

It became clear from the large variety of experimental and computational studies that the environment surrounding LeuT and the NSS transporter proteins can play a critical role in their function (Quick et al., 2012; Wang et al., 2012). Combined with the observation of significant reorientations of TM segments and their direct relation to the functional mechanism (Zhao et al., 2010, 2011), we reasoned that a quantitative evaluation of the membrane–protein interaction patterns is essential in order to understand the functional mechanisms of these important proteins. As part of this study, we present here the results of a quantitative evaluation of the nature and effects of membrane–protein interactions for LeuT, in the context of different conformations associated with the transport mechanism.

We present the results from calculations of membrane deformation and residual exposure profiles using the CTMD approach applied first to published molecular dynamics trajectories of LeuT in its key conformational states (Shi et al., 2008; Zhao et al., 2010), viz., outward-open, occluded, and inward-open states and embedded in a 1-palmitoyl-2-oleoyl-sn-glycero-3-phosphocholine (POPC) lipid bilayer. The analysis identified strikingly large effects at the membrane–protein interface, including thinning of the membrane and a large extent of water penetration into a region of the membrane bilayer near the membrane-facing polar residue K288 of TM7. Notably, hydrophobic residues of TM7 and the TM1a segment of TM1 positioned in the neighborhood of K288 were found to be exposed to this water penetration due to their relatively large residual exposure at the deformed membrane–protein boundary.

The membrane-facing lysine at position 288 in LeuT is not a conserved residue in the NSS, and the special properties of the membrane environment of LeuT in the bacterial cell might

Table 1
Molecular constructs studied with MD simulations.

PDB code	3F3A			3GJD		3GJD-K288A
Constructs[a]	S1 – Trp S2 – ⌀[b]	S1 – Trp S2 – Trp	S1 – Trp S2 – Trp, OG, C14[c]	S1 – Leu S2 – ⌀	S1 – Leu S2 – OG	S1 – Leu S2 – ⌀
Time (ns)[d]	95	89	104	96	87	113
N_{POPE}	534	534	534	534	534	534
N_{POPG}	161	161	161	160	160	160
N_W	58,541	58,541	58,541	57,529	57,529	57,367
N_{Cl-}	6	6	6	5	5	4
N_{Na+}	159	159	159	158	158	158

[a] 3F3A structure contained $2Na^+$ ions, and 3GJD had $2Na^+$ and $1Cl^-$ ions, all retained in MD simulations.
[b] ⌀ denotes empty S2 site.
[c] S2 site contains TPR, OG and C14.
[d] Production run, excludes equilibration phase.

affect the specific effects calculated in the POPC lipid bilayer, a common membrane model in the computational study of mammalian membrane proteins. Therefore, we investigated whether the large residual exposures we observe in the neighborhood of K288 occur as well in an environment more similar to the bacterial membrane. To this end we repeated the analysis for a LeuT embedded in the more native-like 3:1 1-palmitoyl-2-oleoyl-sn-glycero-3-phosphoethanolamine (POPE)/1-palmitoyl-2-oleoyl-sn-glycero-3-phosphoglycerol (POPG) lipid mixture, with MD trajectories starting from different crystal structures, viz., 3F3A and 3GJD (a complete list of molecular dynamics trajectories in this paper is given in Table 1 of Section 2). The remarkable residual exposure was found as well in the more native-like membrane. It became important, therefore, to consider the functional effect of this significant perturbation of the membrane-facing polar lysine residue at position 288 of LeuT, in view of experimental data showing that a K288A mutant exhibits improved transport properties in experimental systems (Piscitelli and Gouaux, 2012; Piscitelli et al., 2010). The results obtained for the K288A mutant construct verified that the effect at the neighboring hydrophobic residues is due to the interaction of the polar K288 with the membrane. Thus, the mutation abolished the large membrane deformation near K288A and also the residual exposure at the neighboring hydrophobic residues of TM1a and TM7. These findings, and the experimentally demonstrated effect of the K288A mutation on the transport efficiency of LeuT, led to the proposal of a mechanism by which the characteristics of the K288 involvement in the local protein–membrane interaction affect the rate of transition to the inward-open state of the transporter.

2. Methods

2.1. Continuum-Molecular Dynamics (CTMD)

The recently described hybrid Continuum-Molecular Dynamics (CTMD) approach (Mondal et al., 2011) was employed here to quantify membrane deformations around LeuT and corresponding energetics, as well as residual exposure, i.e., the hydrophobic mismatch at specific residues that is not alleviated by membrane deformations. To evaluate these quantities, the membrane–protein interface is first described at an atomistic level with Molecular Dynamics (MD) simulations, and the corresponding membrane deformations are then calculated at the continuum level with the elastic theory of membrane deformations but without making the typical assumption of cylindrical symmetry (Andersen and Koeppe, 2007; Nielsen et al., 1998). In the process, the continuum-level calculations yield as well the energy cost of these membrane deformations. The CTMD approach is available as part of the stand-alone application $CTMD_{app}$ at http://memprotein.org/resources/servers-and-software.

For this study, we present an extension of the previously described CTMD approach in order to take into account the significant asymmetry in the lipid–protein interactions in the two leaflets discussed for transporters like LeuT (Pantano and Klein, 2009). While it has been a common approximation to consider bilayer deformations as an average over the two leaflets (Mondal et al., 2011; Nielsen et al., 1998), the two leaflets of the bilayer can be treated separately at the continuum-level (Callenberg et al., 2012; Huang, 1986; Khelashvili et al., 2009b), and here we describe an extension of CTMD that treats the two leaflets of the bilayer separately.

2.1.1. Membrane deformations

The membrane shape is described in terms of the local deformations $u_+(x,y)$ and $u_-(x,y)$ of the upper and lower leaflet, respectively:

$$u_+(x,y) = d_+(x,y) - 0.5 * d_0, \tag{1a}$$

$$u_-(x,y) = d_-(x,y) - 0.5 * d_0, \tag{1b}$$

where d_0 is the "bulk" bilayer thickness away from the protein, and $d_+(x,y)$ and $d_-(x,y)$ are the local bilayer heights of the upper and lower leaflet, respectively, defined relative to the mid-plane.

With contributions from compression–extension, splay–distortion, and surface tension terms (Huang, 1986; Mondal et al., 2011; Nielsen et al., 1998), the energy cost of bilayer deformations is

$$\Delta G_{def} = \frac{1}{2}\int_{\Omega}\left\{K_a\frac{(u_+ - u_-)^2}{{d_0}^2} + \frac{1}{2}K_c[(\nabla^2 u_- - {C_0}^2)^2 + (\nabla^2 u_+ - {C_0}^2)^2] + \frac{1}{2}\alpha[(\nabla u_+)^2 + (\nabla u)^2]\right\}d\Omega, \tag{2}$$

where Ω represents the membrane area, K_a is the compressibility modulus, K_c is the bending modulus, α is the coefficient of surface tension, and C_0 is the monolayer spontaneous curvature (for parameterization details see Section 2.4 below).

To determine $u_+(x,y)$, $u_-(x,y)$, and the corresponding ΔG_{def}, the two leaflets were treated as uncoupled in the solution procedure (Callenberg et al., 2012). Specifically, to solve for $u_+(x,y)$, we set $u_-(x,y) = 0$ in Eq. (2). Similarly, to solve for $u_-(x,y)$, we set $u_+(x,y) = 0$ in Eq. (2). Following this simplification, the deformations were determined separately in the two leaflets by minimizing

the corresponding ΔG_{def}. Specifically, $u_+(x,y)$ and $u_-(x,y)$ were obtained by solving the corresponding Euler–Lagrange equations:

$$\begin{aligned} &K_c\nabla^4 u - \alpha\nabla^2 u + \frac{2K_a}{{d_0}^2}u = 0, \\ &u|_{\Gamma in} = u_0(x,y); u|_{\Gamma out} = 0 \\ &\nabla^2 u|_{\Gamma in} = v_0(x,y); \nabla^2 u|_{\Gamma out} = 0 \end{aligned} \quad , \tag{3}$$

where the generic notation u is used to represent $u_+(x,y)$ and $u_-(x,y)$, in the respective equations, Γ_{in} represents the membrane–protein boundary, and Γ_{out} is the outer boundary contour in the bulk.

The boundary value problem in Eq. (3) is solved numerically without assuming cylindrical symmetry of membrane deformations, according to the procedure described in the original CTMD formulation (Mondal et al., 2011). To this end, Γ_{in} and the boundary conditions for $u(x,y)_+$ and $u(x,y)_-$ at Γ_{in} were obtained from atomistic MD simulations of the system. To obtain these boundary conditions, the membrane surface was first represented on a rectangular grid with spacing of 2 Å that was fit to the phosphates of each leaflet in the cognate MD trajectories and centered at the transmembrane protein. The gridded data was then time-averaged and spatially smoothed. The smoothing represents the scaling step between MD and continuum-level calculations. It ensures that there are no large jumps in the gridded data at individual gridpoints at the membrane–protein interface, so that the gridded data obtained from microscopic-level MD calculations can be used as boundary condition in the subsequent continuum-level calculations. The smoothing is performed by spatial averaging, i.e., the value at gridpoint (i,j) is iteratively computed as the average of the values at gridpoints (i,j), $(i+1,j)$, $(i-1,j)$, $(i,j-1)$, and $(i,j+1)$, ignoring a gridpoint if it is not populated (Mondal et al., 2011). In defining the membrane–protein boundary from this gridded data, grid squares at the interface are considered only if they were populated by phosphates in both leaflets. The corresponding $u_{+,MD}(x,y)$ and $u_{-,MD}(x,y)$, calculated with Eq. (1) from the grid, provide the boundary condition $u_0(x,y)$ at Γ_{in} for each leaflet, respectively. The boundary condition on curvature at Γ_{in}, i.e., $v_0(x,y)$, was determined by means of a self-consistent optimization procedure that minimizes ΔG_{def} as detailed in the original description of the CTMD method (Mondal et al., 2011). We note that the membrane deformations obtained after this optimization procedure at the continuum level agreed with the corresponding deformations obtained directly from the microscopic MD trajectories (Fig. S1).

2.1.2. Residual exposure

The residual exposure of protein residues at the membrane–protein interface was quantified from the calculation of the surface area $SA_{res,i}$ of hydrophobic residues exposed to polar environment, and of polar residues embedded in hydrophobic environment, in the MD trajectories. The corresponding energy cost $\Delta G_{res,i}$ for each residue was calculated as a linear function of the residual exposure area $SA_{res,i}$:

$$\Delta G_{res,i} = \sigma_{res} SA_{res,i} \tag{4}$$

with the constant of proportionality σ_{res} taken to be 0.028 kcal/(mol Å^2) (Ben-Tal et al., 1996; Choe et al., 2008). Further methodological details are available in (Mondal et al., 2011).

2.2. Molecular constructs

The atomistic MD simulations have been carried out on molecular constructs of LeuT (see Table 1) from two different X-ray structures: PDB accession codes 3F3A (Singh et al., 2008) and 3GJD (Quick et al., 2009). In the outward-facing 3F3A structure, LeuT contains a Trp molecule in the primary binding site S1, and the molecules Trp, β-octylglucoside (OG) detergent, and tetradecane (C14) in the secondary binding site (the S2 site). In the occluded structure, 3GJD, the transporter is complexed with Leu in the S1 site, and OG in the S2 site. Several MD simulations were carried out on constructs differing in the content of their S2 site, as detailed in Table 1.

For the starting structures, LeuT residues that were missing from the X-ray structure were added with Modeller (Sali and Blundell, 1993); these included in 3F3A the first 4 residues on N-terminus, and residues N133–A134 in EL2 loop; in 3GJD the first 4 residues of the N-terminus, the last 8 residues of the C-terminus, and the P132–N133–A134 stretch in the EL2 loop. All crystallographic waters and ions were retained in the simulations. Residues Glu112, Glu287, and Glu419 were protonated.

To obtain the Lys288-to-Ala (K288A) mutant construct, the substitution was carried out in the 3GJD structure of LeuT using VMD (Humphrey et al., 1996). All LeuT models from Table 1 were inserted in a pre-assembled lipid membrane model that was composed of a 3:1 mixture of POPE (1-palmitoyl-2-oleoyl-sn-glycero-3-phosphoethanolamine) and POPG (1-palmitoyl-2-oleoyl-sn-glycero-3-phosphoglycerol) (see Table 1 for the number of lipids), a mixture that is closely related to *Escherichia coli* lipid extract (Raetz, 1978). This lipid bilayer was built using the CHARMM-GUI web facility (Jo et al., 2009). After protein insertion and upon removal of overlapping lipids, the LeuT/membrane complex was solvated with TIP3 waters and then ionized with Na^+ and Cl^- to achieve an ion concentration of 0.15 M.

Conformations of LeuT corresponding to the outward-open, occluded, and inward-open states have been simulated previously in model POPC membrane with various combinations of regular and steered MD simulations (for details, see Shi et al., 2008; Zhao et al., 2010, 2011). The atomistic trajectories for these conformations were also used here for the CTMD calculations described in Section 2.1.

2.3. Molecular dynamics simulations

All-atom MD simulations were carried out with the NAMD 2.7 package (Phillips et al., 2005) using all-atom CHARMM force fields: CHARMM27 with CMAP corrections for proteins (Brooks et al., 2009), CHARMM36 lipid force field (Klauda et al., 2010), and CHARMM-compatible force-field parameter set for OG detergent derived from that of *N*-dodecyl-β-maltoside detergent (Abel et al., 2011). Molecular constructs were first equilibrated for 5 ns according to the protocol previously developed in our lab (Shi et al., 2008). According to this protocol, the transporter backbone and the heavy atoms of the substrates bound in the S1 and S2 sites were initially fixed and then harmonically constrained to prevent water penetration. Constraints were released gradually with decreasing force constants of 1, 0.5, and 0.01 kcal/(mol Å^2). After this initial equilibration phase, unbiased MD simulations were carried out (Table 1) with an integration step of 1 fs for the equilibration stage and 2 fs thereafter, in an NPT ensemble under semi-isotropic pressure coupling conditions and at 310 K temperature; PME was used for electrostatics interactions. The Nose–Hoover Langevin piston algorithm was used to attain the target 1 atm pressure with the LangevinPistonPeriod set to 100 fs and LangevinPistonDecay set to 50 fs. Because this article reports, to our knowledge, the first MD simulation of the biologically important ~3:1 mixture of POPE and POPG lipids with the C36 force field, we report in Fig. S2 of the supplementary material the deuterium order parameters of lipid tails for POPE and POPG at a sufficient distance (>20 Å) away from the protein (this is possible here because we used a large membrane patch of POPE/POPG), so that relatively far from the protein (>20 Å) there were ~100 POPG lipids and ~350 POPE lipids available for

Table 2
Residual exposure energy penalty (kT) of LeuT in POPC lipid bilayer. Only TMs with energy cost > 1 kT at one or more membrane-facing residues are shown.

Residue	Outward-facing	Occluded	Inward-facing
TM1	3.3	3.1	3.4
TM7	3	3.4	2.9
TM11	2	3.1	2.6

the calculation of order parameters. As detailed in the caption of Fig. S2, the order parameters calculated here are consistent with available spectroscopic and simulation data in the literature.

2.4. Parametrization of the CTMD model

The continuum equations for membrane deformations (Eq. (3)), when applied to LeuT in the POPC bilayer, were solved with the following macroscopic elastic parameters for POPC lipid: $K_a = 230\,mN/m$ (Rawicz et al., 2000), $K_c = 8.5 \times 10^{-20}\,J$ (Kucerka et al., 2006), $\alpha = 3 \times 10^{-13}\,N/Å$ (Nielsen et al., 1998), $C_0 = 0$ (Soubias et al., 2010), and a phosphate-to-phosphate bilayer thickness of $d_0 = 42\,Å$ based on the bilayer thickness away from the protein.

For LeuT in the 3:1 POPE/POPG lipid mixture, we did not carry out ΔG_{def} energy calculations due to the lack of experimental estimates for C_0 of POPE and POPG lipids. An estimate for C_0 of DOPG has been used recently as a proxy for the C_0 of POPG (Strandberg et al., 2012), and that of DOPE – for POPE (Marsh, 2007). However, we do not report energy costs for the POPE/POPG mixture calculated with the available experimental estimates for C_0 of DOPE/DOPG lipid mixtures (Alley et al., 2008), because the quadratic nature of the curvature energy term renders the energy cost of membrane deformations highly sensitive to the large C_0 values of DOPE or POPE rich lipid mixtures. In any case, calculating this energy cost for the POPE/POPG lipid bilayer was not necessary in order to reach the conclusions in this paper.

3. Results

3.1. Hydrophobic mismatch between LeuT and a POPC bilayer is not completely alleviated by membrane deformations

To obtain a quantitative description of the interaction of LeuT with its membrane environment in the context of the transport mechanism of LeuT, we applied the recently described hybrid Continuum-Molecular Dynamics (CTMD) approach (Mondal et al., 2011) to LeuT in its three known conformations in the transport cycle viz. outward-open, occluded, and inward-open conformations. For these calculations, we took advantage of available trajectories from our reported atomistic Molecular Dynamics (MD) simulations of LeuT embedded in POPC lipid bilayer (Claxton et al., 2010; Shi et al., 2008; Zhao et al., 2010, 2011) to characterize the membrane–protein interface as described in Methods.

Analysis of the hydrophobic mismatch revealed that specific membrane-facing residues in TM1, TM7, and TM11 remain exposed to unfavorable hydrophobic-polar interactions with energy penalty >1 kT in all three conformations (Fig. 1 and Table 2). The general reasons for incomplete alleviation of hydrophobic mismatch in multi-TM proteins have been discussed elsewhere (Mondal et al., 2011). In the LeuT system, the residues exhibiting residual exposure in all three conformations of the protein are L12 in TM1a (the cytoplasmic segment of TM1), L277 of TM7, and P473 of TM11; the I15 residue in TM1a is exposed only in the inward-facing conformation. The energy cost of residual exposures is evaluated to be 2–3.5 kT per residue (Table 2). Note that here we only consider the residual exposure at membrane-facing residues. Interestingly, the residual exposure occurs even though the hydrophobic thickness of the POPC bilayer is well matched to the average hydrophobic thickness of LeuT. Specifically, we have verified this by using the Orientations of Proteins in Membrane (OPM) utility PPM 2.0 (Lomize et al., 2011, 2006) to position a LeuT monomer (from various X-ray crystal structures) in a uniform hydrophobic milieu of adjustable thickness. From this procedure we obtained an average hydrophobic thickness of ~27–28 Å with a precision of <~2 Å (see Fig. S3). This value is well-matched to the experimental estimate of ~27 Å for the hydrophobic thickness of POPC bilayer (Kucerka et al., 2006).

To understand why complete hydrophobic matching is not achieved between the POPC bilayer and the embedded LeuT molecule, we examined the structural context of the residues exhibiting large residual exposure (Fig. 1A and B) and found them to be adjacent to residues of opposite hydrophobic character. Specifically, the hydrophobic L12 of TM1a and L277 of TM7 are both adjacent to the membrane-facing polar K288 of TM7 (Fig. 1A), and the hydrophobic P473 of TM11 is adjacent to the polar R469 (Fig. 1B). The consequences of these adjacencies for the interaction with the membrane are evident from the results of the MD simulations, as illustrated with snapshots from the trajectories in Fig. 1A and B. We find that although the lipid-facing K288 is immersed deep within the membrane (three helical turns above the cytoplasmic end of TM7), the deformation of the membrane enables it to interact with a polar environment of water and lipid head-groups due to a dramatic bending of the phospholipid surface and water penetration (Fig. 1A). As a result of the hydrophobic matching at K288, the neighboring hydrophobic residues L12 and L277 can no longer be completely covered by the hydrophobic core of the lipid bilayer and become unfavorably exposed to the polar environment (Fig. 1A), thus incurring a substantial energy penalty (Table 2).

Interestingly, the residual exposure at L12 in the inward-facing conformation is smaller (1.4 kT) than that in the outward-facing or occluded states (~3 kT, see Fig. 1C). This correlates with a relative motion of the TM1a segment away from the protein bundle and into the membrane when LeuT transitions from the occluded to the inward-facing conformation. However, this re-positioning of TM1a brings another K288-juxtaposed hydrophobic residue in TM1a, I15, into a membrane-facing position adjacent to the thinned area of the membrane near TM7 (see Fig. 1A). The calculations show that the energy cost of residual exposure of I15 is ~2 kT in the inward-facing state of LeuT (Fig. 1C), so that the combined energy penalty at TM1 is ~3–3.5 kT in the inward-facing state as well (Table 2).

Another membrane-facing residue involved in unfavorable polar–hydrophobic interactions is P473 of TM11 (Fig. 1B and C). Using the OPM-based analysis of degrees of residual exposure in membrane models of different uniform thickness, as described above, we concluded that the accessibility of P473 involves lipid–protein interactions (Fig. S5), even if this residue is also partly accessible to water from the extracellular vestibule. Specifically, we embedded the LeuT structure PDBid 3F3A in slabs of increasing thickness and found that P473 can be accommodated inside the hydrophobic core by a modest thickening in the upper leaflet (to a hydrophobic thickness of 30.8 Å for the bilayer). Because this membrane deformation, which would have alleviated the hydrophobic mismatch at P473 does not occur in POPC (Fig. 1C), we reason that the nearby presence of an embedded R469 (see Fig. S5) has made this too costly energetically. Thus, Fig. S5B shows R469 is likely too far away (more than 8.2 Å in the Z-direction alone from the phosphates) to alleviate the hydrophobic mismatch by snorkeling alone. Taken together, these observations identify the accessibility at P473 as another example of residual exposure, resulting in substantial energy penalty (2–3 kT, see Table 2) that is still lower than what a buried arginine would incur (see, for example, Moon and Fleming, 2011). Consistent with this reasoning, a local thinning of the POPC lipid bilayer is observed to occur near TM11 (Fig. 2).

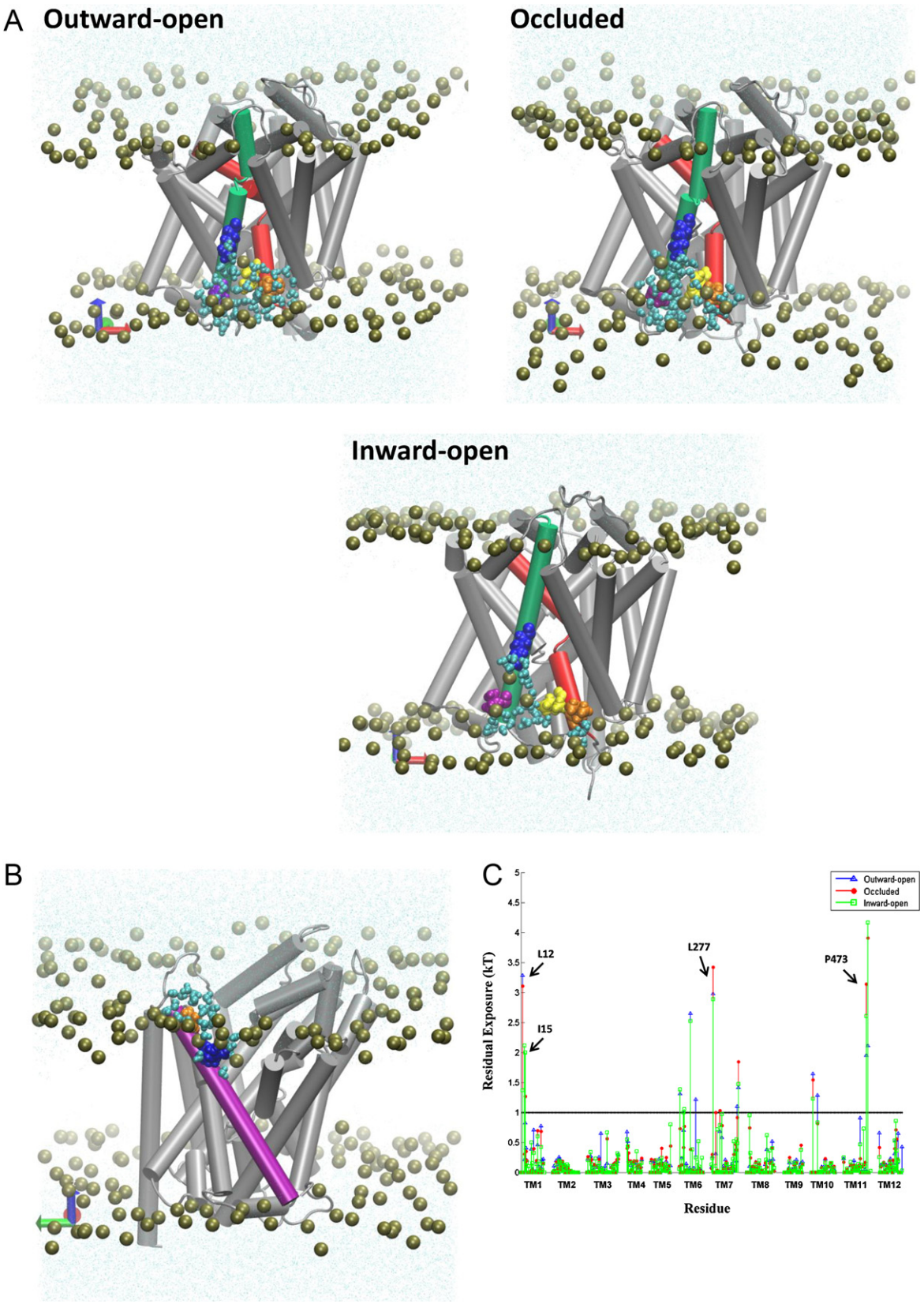

Fig. 1. Residual exposure in a POPC lipid bilayer of LeuT residues in the three conformational states. (A) Lipid–water–protein interactions at TM1 (in red) and TM7 (green) in snapshots from the atomistic MD trajectories for the outward-open, occluded, and inward-open conformations of LeuT. The highlighted residues are K288 (blue), L277 (purple), L12 (orange), and I15 (yellow). Water molecules within 5 Å of these residues are shown in cyan CPK representation. The membrane is indicated by the phosphates of the two leaflets, shown in tan color. (B) Snapshot from the atomistic MD trajectory for the outward-open conformation, illustrating lipid–protein interactions at TM11 (purple). The highlighted residues are P473 (orange) and R469 (blue). Water molecules within 5 Å of these residues are shown in cyan CPK representation, and the bilayer phosphate headgroups in tan. (C) Energy penalty due to residual exposure (in kT units) of LeuT residues in the outward-open (blue), occluded (red), and inward-open (green) conformations. Energy costs are shown only for residues in the TM-bundle. For reference, the energy costs calculated for all residues in the outward-facing conformation are available in Fig. S4 of the supplementary data.

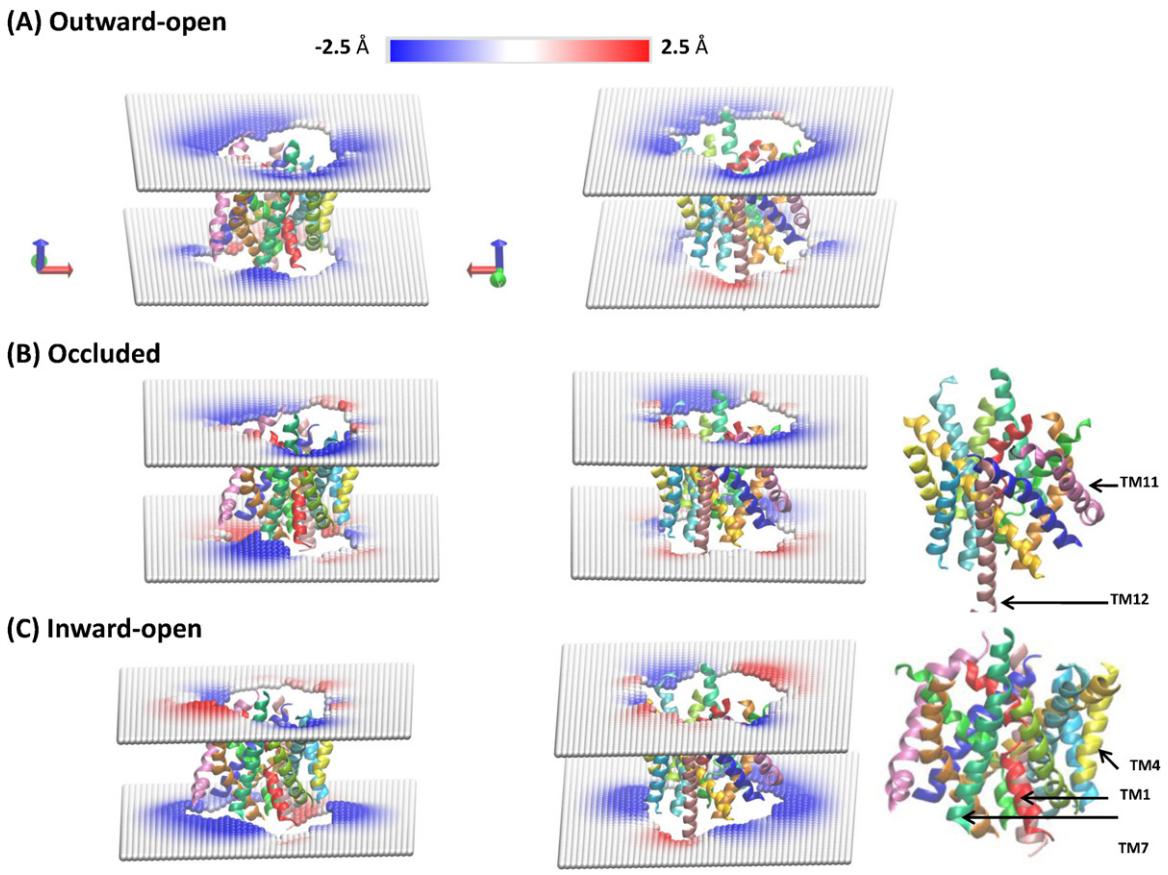

Fig. 2. Local deformations of the upper and lower leaflets of the POPC lipid bilayer around LeuT in its (A) outward-open, (B) occluded, and (C) inward-open conformations. The membrane deformation profiles for each conformation are shown from two different angles (right and left columns), and the TM-bundle of the protein is shown to provide a frame of reference for the membrane deformations. The deformations were calculated for each leaflet with the CTMD approach on a (100 Å × 100 Å) grid with a spacing of 2 Å. Only regions of the bilayer with lipids in both leaflets were considered in the continuum calculations, effectively removing phospholipids interacting with the protein as individual molecules.

The bending of the phosphate surface observed locally from the results of MD simulations is, of course, a component of the global membrane deformation profile. To quantify this profile and its corresponding energetics, we calculated the equilibrium shapes of the POPC membrane leaflets around LeuT with the hybrid CTMD approach (see Section 2). The deformation profiles (Fig. 2) show the bilayer thinning near TM7 and TM11 in all three conformations of the transporter (blue colors in Fig. 2). But in addition, Fig. 2 reveals other regions of local thinning and thickening around LeuT. For example, considerable thinning occurs near the cytoplasmic ends of TM4 and TM5, and a thickening of the membrane occurs near TM9 and TM12 (Fig. 2).

3.2. The complicated radial asymmetry of local membrane thickening and thinning of the membrane is essential for relieving hydrophobic mismatch in multi-TM proteins

While not all the complex hydrophobic mismatch pattern can be eliminated by membrane deformation, as shown above, the extent to which local membrane thickening and thinning in the POPC bilayer relieves the hydrophobic mismatch between the protein and the membrane, becomes evident when the results are compared to the LeuT residues that are seen in the OPM slab to be unfavorably exposed (Fig. S3A–C). Considering that the OPM slab represents the best matching of a hydrophobic milieu of uniform thickness to LeuT, the significant unfavorable exposure still remaining at several residues in LeuT indicates that radially symmetric membrane deformations do not suffice to alleviate the hydrophobic mismatch of LeuT. However, we find that in MD-based calculations, most of these residues are accommodated in the locally deformed POPC bilayer (Figs. 1C, 2 and S3D), indicating a general tendency towards hydrophobic matching by means of local membrane deformations. For example, the hydrophobic residues F502 and L503 in TM12 are accommodated within the hydrophobic core of the locally thicker POPC membrane (Fig. S3D). Finally, as mentioned above, the local membrane thinning in the lower (cytoplasmic) leaflet near TM7 accommodates the polar K288, and that in the upper leaflet near TM11 accommodates R469 (see Section 2 for a description of separate leaflet calculations).

It is evident from Fig. 2 that the extent of these membrane deformations is different in the outward-open, occluded, and the inward-open conformations. To investigate if the different extents of deformation involve a substantial difference in energy costs as well, we quantified the energy cost of membrane deformations for the three conformations. The deformation energies (calculated relative to a flat bilayer state) were 3.9 kT in the inward-facing conformation and 3.1 kT in both the outward-open and the occluded conformation. Taken together, our quantitative analysis of membrane deformations and the residual exposure in the POPC model membrane reveals that the deformations around LeuT tend to reduce hydrophobic mismatch between the protein and the membrane. The membrane deformation energies are similar in the three conformations and do not appear to be important in differentiating the conformational states energetically. But the hydrophobic mismatch is not completely alleviated by membrane deformations in any of the three states of the transporter. The energetically costly residual exposures occurring at TMs 1, 7, and 11 may play a role in the transitions among functionally distinct conformations, as

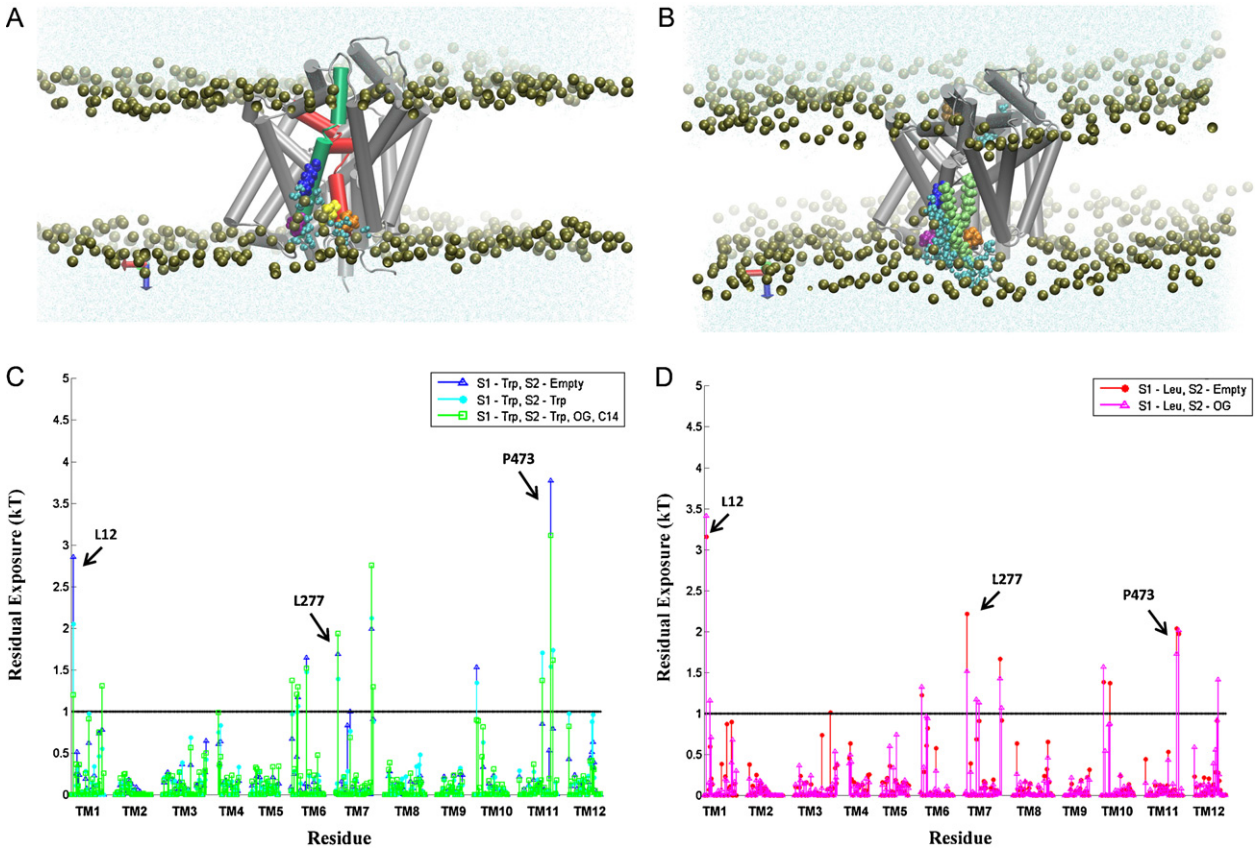

Fig. 3. Residual exposure of LeuT residues in a native-like 3:1 POPE/POPG lipid bilayer. (A) Snapshot from the atomistic MD trajectory for the outward-open conformation stabilized by Trp bound to the primary and secondary binding sites S1 and S2 (based on PDB 3F3A), illustrating the lipid–protein interactions at TM1 (red) and TM7 (green). The highlighted residues are K288 (blue), L277 (purple), L12 (orange), and I15 (yellow). Water molecules within 5 Å of these residues are shown in cyan CPK representation, with the phosphates of the two leaflets shown in tan. Trp in S1 and S2 sites are omitted for clarity. (B) Snapshot from the atomistic MD trajectory with OG and C14 detergents bound in the S2 site. The single lipid molecule shielding L12 from water molecules is highlighted in lime color. The detergent OG is highlighted in ochre color to show its position relative to K288. Waters and membrane phosphates are shown as in (A). Trp-s in S1 and S2 sites as well as C14 in S2 site are omitted for clarity. (C) Energy penalty due to residual exposure for the outward-open conformation of LeuT (based on PDB 3F3A) with Trp in the S1 site only (in blue), or with Trp in both S1 and S2 sites (cyan), or with the OG and C14 detergent molecules in S2, along with Trp in S1 and S2 (green). Energy costs are shown only for residues in TM segments. (D) Energy penalty due to residual exposure in the occluded conformation of LeuT (based on PDB 3GJD), with Leu bound in S1 (red), or with Leu in S1 and an OG detergent molecule in S2 (magenta). Energy costs are shown only for residues in TM segments.

discussed further below in the comparison between the WT and K288A constructs.

3.3. The residual exposures at TMs 1, 7, and 11 are retained in the native-like environment of the 3:1 POPE/POPG bilayer

In the POPC lipid bilayer, which is a standard membrane model in theoretical and experimental studies of membrane proteins, the residual exposure was found to occur at TMs 1, 7, and 11 of LeuT in several different conformations. While the POPC bilayer is reasonably well matched with LeuT in terms of average hydrophobic thickness, LeuT functions in bacterial membranes, and bacterial membranes are rich in a mixture of phospholipids with PE and PG headgroups, rather than the PC headgroup (Dowhan, 1997). To investigate whether the residual exposure at the identified sites of LeuT changes in this more native-like membrane environment, we repeated the calculations of residual exposure for LeuT embedded in a 3:1 POPE/POPG lipid bilayer, a lipid composition that has been used to model the inner bacterial membrane (Murzyn et al., 2005).

Fig. 3 shows the residual exposure for the residues in the TM-bundle of LeuT, calculated from MD trajectories that were initiated from the outward-open conformation of the wild type transporter stabilized with the competitive transport inhibitor Trp (PDB 3F3A (Singh et al., 2008), Table 1). In the 3F3A X-ray structure, one Trp is bound in the primary S1 binding site, and another in the secondary S2 site in the extracellular vestibule of LeuT. For conformations with Trp bound in both S1 and S2, as well as for conformations with Trp bound only in the S1 site, our calculations show a residual exposure of >1 kT at L12 of TM1 (2–3 kT) and L277 at TM7 (1–2 kT) – see Fig. 3C and Table 3. Similar to the results for POPC, the residual exposures at these locations are found here to be associated with the bending of the phosphate surface towards the positively charged K288 residue in TM7 and water penetration in the region (Fig. 3A). A residual exposure of >1 kT was also found for P473 of TM11, similar to that seen in POPC membrane. These calculations confirm that the residual exposure pattern at the hydrophobic residues near K288 and R469 residues found for LeuT embedded in POPC membranes occurs as well in the more native-like 3:1 POPE/POPG lipid environment. To assess the effect of substrate-determined conformations we calculated the residual exposures as well from MD trajectories starting from the Leu-bound 3GJD X-ray structure (Quick et al., 2009) (Table 1) that represents an occluded state of LeuT with a Leu in S1. The results for the residual exposure energies are presented in Fig. 3D and Table 3. Here too, the residues with residual exposure that have an energy penalty >1 kT are L12 in TM1a and L277 of TM7, resulting in totals of 3.2 kT for TM1a, and 2.2 kT for TM7. In agreement with the mechanistic explanation identified in the POPC membrane, this residual exposure is associated with bending of the phosphate surface and water penetration near K288 accessing membrane-facing residues that would otherwise not be exposed.

Table 3
Residual exposure energy penalty (kT) of LeuT in the POPE/POPG (~3:1) lipid bilayer. Only TMs with energy cost > 1 kT at one or more membrane-facing residues are shown.

PDB ID	3F3A			3GJD		3GJD (K288A)
Constructs[a]	S1 – Trp S2 – ⌀[b]	S1 – Trp S2 – Trp	S1 – Trp S2 – Trp, OG, C14[c]	S1 – Leu S2 – ⌀	S1 – Leu S2 – OG	S1 – Leu S2 – ⌀
TM1	2.9	2	1.2	3.2	3.4	1.1
TM7	1.7	1.4	1.9	2.2	1.5	0.2
TM11	3.8	1.5	3.1	2	1.7	1.4

[a] See Section 2 for details of each construct.
[b] ⌀ denotes empty S2 site.
[c] S2 site contains TRP, OG, and also a tetradecane (C14) similar to the crystal structure.

The presence of the detergent molecule octylglucoside detergent (OG) in the extracellular vestibule of both 3F3A and 3GJD crystal structures has been identified as a factor in the stabilization of an inactive (inhibited) conformation of LeuT (Quick et al., 2009). Therefore, we investigated the lipid–protein interactions in the context studied here for the LeuT conformation in the presence of OG. Fig. 3C and D compares the calculated residual exposure energies in the Trp-bound and Leu-bound constructs, in the presence or absence of OG molecule in S2 site. Interestingly, for the Trp-bound outward-facing conformation (based on 3F3A) our calculations do report a smaller residual exposure at residue L12 in the OG-bound state. However, from an examination of the trajectories, this does not appear to be related to the interactions in the S2 site where OG is bound. Rather, in this MD trajectory a POPE lipid molecule is interposed between the penetrating water near K288 and the neighboring L12, shielding L12 from unfavorable interactions with the penetrating water (Fig. 3B). Moreover, the energy penalty of the residual exposure at L277 is more than 1 kT in this case as well. For the occluded conformation (3GJD), the calculations with and without OG show comparable residual exposure at TMs 1, 7, and 11. Taken together, our data do not show an effect of the detergent molecule in S2 site on the residual exposure energies in either open-outward or occluded states of LeuT.

3.4. In silico K288-to-Ala mutation abolishes residual exposure at L12 and L277

To establish the relation between the effect seen on the residual exposure of the non-polar residues L12 (TM1a) and L277 (TM7), and the role of the adjacent polar residue K288 (TM7), we conducted the CTMD calculations on the occluded conformation of LeuT (containing substrate Leu in S1, 3GJD) in which K288 was mutated to Ala (K288A). The substantial membrane thinning and associated water penetration reported for the wild type transporter in Section 3.3 are not observed for the mutant, as illustrated in a snapshot of the trajectory in Fig. 4A. As expected, the residual exposure profile showed that in the K288A construct the residual exposure at L12 is reduced from ~3 kT to ~1 kT, and at L277 from ~2.2 kT to <1 kT (Fig. 4B and Table 3). We also note that the residual exposure at P473 of TM11, the residue at an approximately diametrically opposite side of the mutation site, remains high in the K288A construct (Table 3). Thus, the K288A mutation has a dramatic effect on the residual exposure energies for the specific hydrophobic residues adjacent to the site of the mutation. This substantiates the mechanism we propose, in which the local effects on residual mismatch are produced by adjacency to residues with diverse polarity – a relatively common occurrence in multi-TM membrane proteins.

4. Discussion

The membrane environment of the prototypical neurotransmitter transporter analog LeuT is shown from the results presented here to respond dynamically to the structural features and conformational changes related to functional states of this transmembrane protein. That the energetics of this type of membrane remodeling are significant for the function and organization of proteins in the cell membrane has been established previously for the GPCRs (Botelho et al., 2002, 2006; Brown, 1994; Mondal et al.,

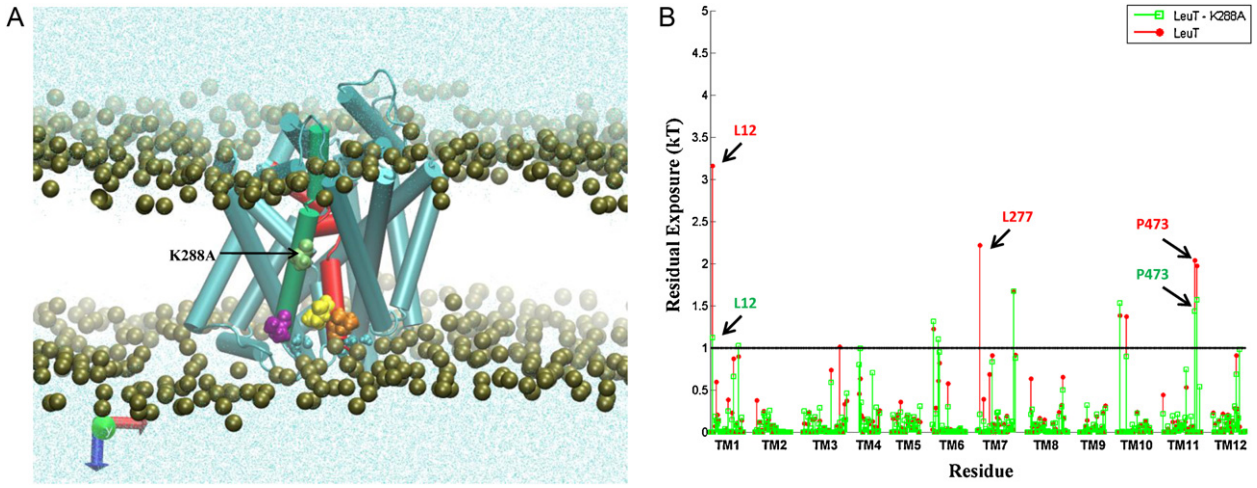

Fig. 4. Residual exposure is reduced in the Lys288-to-Ala mutant. (A) Snapshot from the atomistic MD trajectory for the K288A mutant (based on PDB 3GJD) in a ~3:1 POPE/POPG lipid bilayer, illustrating the lipid–protein interactions at TM1 (red) and TM7 (green). The key residues A288 (lime), L277 (purple), L12 (orange), and I15 (yellow) are highlighted in CPK rendering, and water molecules within 5 Å of these residues are shown (cyan, CPK representation). (B) Comparison of the energy penalty due to residual exposure in the K288A mutant (green) and wild-type LeuT (red), calculated for both in the occluded state with the S1 site occupied by substrate Leu and embedded in a 3:1 POPE/POPG lipid bilayer.

2011, 2012; Periole et al., 2007; Soubias et al., 2010), and for ion channels (Andersen and Koeppe, 2007; Harroun et al., 1999a,b; Huang, 1986; Lundbaek et al., 2003, 2005; Nielsen et al., 1998; Phillips et al., 2009). The calculations we report here show that this energy component resulting from membrane–protein interactions, is important as well for LeuT. Thus, a significant role of the hydrophobic mismatch of LeuT in model membranes is evident from the calculations we report here, which show that both in POPC and in the more native-like POPE/POPG (3:1) bilayers, membrane deformations cannot completely alleviate this mismatch and its energy cost. The residual exposure and its energy penalty were shown to affect specific hydrophobic residues in TMs 1a, 7, and 11 that have a defined spatial relationship with the membrane-facing polar residue K288. We note the involvement of the intracellular end of TM1 (i.e., TM1a) in these unfavorable interactions with the lipid membrane as being especially interesting, because the repositioning of TM1a in LeuT has been shown to be important in the transition from occluded to inward-facing conformations associated with the transport cycle (Krishnamurthy and Gouaux, 2012; Shi et al., 2008; Zhao et al., 2010, 2011).

The residual exposure calculations performed with our recently described hybrid Continuum-Molecular Dynamics (CTMD) approach (Mondal et al., 2011) took into account not only the conformational differences between the functionally defined states of LeuT, but also the dynamic rearrangements of the protein side-chains in the atomistic MD simulations used to describe the membrane–protein interface for the different conformations of LeuT. MD simulation has proved to be of great value in describing such interfacial membrane–protein interactions, e.g., in the studies of lipid association with rhodopsin or contact dynamics between lipids and LeuT (Grossfield et al., 2006; Khelashvili et al., 2009a; Pantano and Klein, 2009; Pitman et al., 2005). In the context of the CTMD framework, the major advantage of MD simulations is that they make it possible to account for the radial asymmetry of the hydrophobic surface of multi-segment proteins in calculating the energetics of membrane deformations and residual exposure, through the use of MD-extracted boundary conditions. The same type of computational analysis applied here to study the LeuT-membrane interaction had previously revealed functionally significant residual exposure in a number of GPCR systems (Mondal et al., 2011, 2012). Indeed, like in LeuT, the multi-TM GPCRs (Mondal et al., 2011) present a heterogeneous hydrophobic surface with polar and hydrophobic residues next to each other at several sites. At these sites, the membrane is under constraint to match different extent of hydrophobic thickness in a neighborhood resulting in the possibility of unalleviated hydrophobic mismatch.

Our results for LeuT show that the residual exposure at hydrophobic residues of TM1 and TM7 ensues from the membrane thinning and water penetration due to the presence in their vicinity of the non-conserved polar residue K288 that faces the membrane. The functional implication of the mechanism that leads to this particular residual exposure is suggested by the experimental data for the transport properties of the K288A mutant. Thus, the LeuT mutant with alanine substituting for K288 was found experimentally to have more than five-fold higher transport efficiency (Piscitelli et al., 2010), so that the K288A construct has been used in both structural and functional studies of LeuT (Krishnamurthy and Gouaux, 2012; Piscitelli and Gouaux, 2012; Piscitelli et al., 2010). Our results, and the dramatic effect of the K288A mutation, suggest that the hydrophobic mismatch at K288 cannot be alleviated by the commonly observed Lys-snorkeling effect (Sankararamakrishnan and Weinstein, 2002; Strandberg and Killian, 2003) alone, because K288 is embedded too deep within the membrane (three helix turns above the cytoplasmic end of TM7, at a distance >∼8 Å length of lysine's stretched side chain that snorkels (Strandberg and Killian, 2003). Evidently, the significant energy cost of burying the cationic residue in the lipid environment is alleviated by the effect of membrane thinning and water penetration near K288, which creates a polar environment from the water and the phospholipid head-groups. However, we show that this process also brings the neighboring L12 and L277 into unfavorable interactions with the polar environment of the penetrating water molecules. In the mutant K288A neither the water penetration nor the membrane thinning are observed near the 288 position, and the residual exposure at L12 and L277 is eliminated as well.

The differences between the WT and K288A observed from experimental studies and our computational results suggest how the K288-related residual exposure profile can impact the function-related conformational change in LeuT from the occluded to the inward-open state. The mechanistic hypothesis suggests that in the WT, the movement of the TM1a segment towards the lipid membrane in the transition to the inward-open state in LeuT would occur in the polar environment produced by water penetration around TM1a, involving hydrophobic residues that would otherwise remain exposed to the lipid membrane. Such a movement is likely to be affected by the energy cost of the residual exposure we described for the hydrophobic L12 and I15. Specifically, the cost of the mismatch is expected to generate a local activation barrier to the movement of TM1a, and thus affect transport. In the K288A mutant this barrier would be reduced (or eliminated) leading to the observed enhancement in transport efficacy.

We note that as surprising as the large and functionally consequential membrane deformation and water penetration near the membrane-exposed polar K288 may seem, such bilayer remodeling has been proposed previously, e.g., from MD studies of an Arg embedded in the membrane core as a part of a model helix (Dorairaj and Allen, 2007). Our results now demonstrate that this remarkable feature occurs as well in a native membrane protein, and identify the mechanism by which it affects functionally relevant properties. Thus, the present analysis of the effect of a membrane-facing polar residue in the prototypical NSS protein LeuT, offers unprecedented insight into the energy-based consequences of the residual exposure that can occur in multi-helical proteins (as opposed to a single TM segment). In such proteins, some residues (e.g., hydrophobic) can become exposed to polarity-mismatched environments due to membrane deformations caused by adjacent mismatched residues (e.g., hydrophilic, as in the case of K288).

The results obtained here from the application of CTMD to LeuT in different conformations of the transport cycle, and embedded in POPC or POPG:POPE (3:1) membranes, can be probed with experimental methods measuring residue accessibility, because water was shown to penetrate not only in the lumen of the translocation path, but also at specifically located hydrophobic residues adjacent to the K288 polar center. For example, an EPR approach used recently to test residue locus accessibility in relation to the functional dynamics in LeuT (Claxton et al., 2010) can be applied to compare solvent accessibilities at L277 and L12 in the wild type and K288A mutant in POPC. The results are expected to offer reliable information about the local effect of membrane–protein interactions at residue K288 and its implication for the membrane deformation effects on the adjacent residues and to guide the refinement of the methods and the interpretation of the results from computations.

The biophysical perspective offered by the conclusions from this work, as well as from previous studies in which the incomplete hydrophobic matching was shown to result from the adjacency of polar and hydrophobic residues in multi-segment membrane proteins, suggest the need to modify the well-known concept of hydrophobic matching (Andersen and Koeppe, 2007; Harroun et al., 1999a; Huang, 1986; Nielsen et al., 1998). Thus, the protein–membrane interaction mechanisms demonstrated here for LeuT and in the previous work on GPCRs (Mondal et al., 2011,

2012; Shan et al., 2012), indicate that the view that residual mismatch arises only from the difference between the average hydrophobic thickness of the protein and the bulk hydrophobic thickness of the membrane (Harroun et al., 1999a,b; Lundbæk and Andersen, 1999; Marsh, 2008) is incomplete. We showed that residual exposure is directly attributable to the radial asymmetry of the hydrophobic surface inherent to multi-segment proteins, and that the residual exposure in LeuT occurs in membrane environments (POPC and 3:1 POPE/POPG) whose unperturbed hydrophobic thicknesses are well-matched to the average hydrophobic thickness of the transporter. Taken together with our previous findings of similar mechanisms of residual exposure in the 7-TM GPCRs, the findings presented here show that the residual exposure is responsible for a critical energy component of membrane–protein interactions that affects both structural and functional properties of membrane proteins with multiple transmembrane segments.

Acknowledgements

This work was supported by the National Institutes of Health grants DA012408 and U54GM087519 to H.W., DA023694 to L.S. Computations were performed on *Ranger* at the Texas Advanced Computing Center (TG-MCB090022), and the Cofrin Center for Biomedical Information of the Institute for Computational Biomedicine at Weill Cornell Medical College. We thank Benoit Roux at the University of Chicago for suggesting a utility to calculate the residual exposures in X-ray structures positioned in the OPM-based hydrophobic milieu, as an extension to our CTMDapp software.

Appendix A. Supplementary data

Supplementary data associated with this article can be found, in the online version, at http://dx.doi.org/10.1016/j.chemphyslip.2013.01.006.

References

Abel, S.p., Dupradeau, F.-Y., Raman, E.P., MacKerell, A.D., Marchi, M., 2011. Molecular simulations of dodecyl-beta-maltoside micelles in water: influence of the headgroup conformation and force field parameters. Journal of Physical Chemistry B 115, 487–499.

Alley, S.H., Ces, O., Barahona, M., Templer, R.H., 2008. X-ray diffraction measurement of the monolayer spontaneous curvature of dioleoylphosphatidylglycerol. Chemistry and Physics of Lipids 154, 64–67.

Amara, S.G., Sonders, M.S., 1998. Neurotransmitter transporters as molecular targets for addictive drugs. Drug and Alcohol Dependence 51, 87–96.

Andersen, O.S., Koeppe, R.E., 2007. Bilayer thickness and membrane protein function: an energetic perspective. Annual Review of Biophysics and Biomolecular Structure 36, 107–130.

Ben-Tal, N., Ben-Shaul, A., Nicholls, A., Honig, B., 1996. Free-energy determinants of alpha-helix insertion into lipid bilayers. Biophysical Journal 70, 1803–1812.

Beuming, T., Kniazeff, J., Bergmann, M.L., Shi, L., Gracia, L., Raniszewska, K., Newman, A.H., Javitch, J.A., Weinstein, H., Gether, U., Loland, C.J., 2008. The binding sites for cocaine and dopamine in the dopamine transporter overlap. Nature Neuroscience 11, 780–789.

Beuming, T., Shi, L., Javitch, J.A., Weinstein, H., 2006. A comprehensive structure-based alignment of prokaryotic and eukaryotic neurotransmitter/Na^+ symporters (NSS) aids in the use of the LeuT structure to probe NSS structure and function. Molecular Pharmacology 70, 1630–1642.

Botelho, A.V., Gibson, N.J., Thurmond, R.L., Wang, Y., Brown, M.F., 2002. Conformational energetics of rhodopsin modulated by nonlamellar-forming lipids. Biochemistry 41, 6354–6368.

Botelho, A.V., Huber, T., Sakmar, T.P., Brown, M.F., 2006. Curvature and hydrophobic forces drive oligomerization and modulate activity of rhodopsin in membranes. Biophysical Journal 91, 4464–4477.

Brooks, B.R., Brooks III, C.L., Mackerell Jr., A.D., Nilsson, L., Petrella, R.J., Roux, B., Won, Y., Archontis, G., Bartels, C., Boresch, S., 2009. CHARMM: the biomolecular simulation program. Journal of Computational Chemistry 30, 1545–1614.

Brown, M.F., 1994. Modulation of rhodopsin function by properties of the membrane bilayer. Chemistry and Physics of Lipids 73, 159–180.

Brown, M.F., Thurmond, R.L., Dodd, S.W., Otten, D., Beyer, K., 2002. Elastic deformation of membrane bilayers probed by deuterium NMR relaxation. Journal of the American Chemical Society 124, 8471–8484.

Callenberg, K.M., Latorraca, N.R., Grabe, M., 2012. Membrane bending is critical for the stability of voltage sensor segments in the membrane. Journal of General Physiology 140, 55–68.

Choe, S., Hecht, K.A., Grabe, M., 2008. A continuum method for determining membrane protein insertion energies and the problem of charged residues. Journal of General Physiology 131, 563–573.

Claxton, D.P., Quick, M., Shi, L., De Carvalho, F.D., Weinstein, H., Javitch, J.A., McHaourab, H.S., 2010. Ion/substrate-dependent conformational dynamics of a bacterial homolog of neurotransmitter:sodium symporters. Nature & Structural Molecular Biology 17, 822–829.

Dorairaj, S., Allen, T.W., 2007. On the thermodynamic stability of a charged arginine side chain in a transmembrane helix. Proceedings of the National Academy of Sciences of the United States of America 104, 4943–4948.

Dowhan, W., 1997. Molecular basis for membrane phospholipid diversity: why are there so many lipids? Annual Review of Biochemistry 66, 199–232.

Goforth, R.L., Chi, A.K., Greathouse, D.V., Providence, L.L., Koeppe, R.E., Andersen, O.S., 2003. Hydrophobic coupling of lipid bilayer energetics to channel function. Journal of General Physiology 121, 477–493.

Grossfield, A., Feller, S.E., Pitman, M.C., 2006. A role for direct interactions in the modulation of rhodopsin by -3 polyunsaturated lipids. Proceedings of the National Academy of Sciences of the United States of America 103, 4888–4893.

Harroun, T.A., Heller, W.T., Weiss, T.M., Yang, L., Huang, H.W., 1999a. Experimental evidence for hydrophobic matching and membrane-mediated interactions in lipid bilayers containing gramicidin. Biophysical Journal 76, 937–945.

Harroun, T.A., Heller, W.T., Weiss, T.M., Yang, L., Huang, H.W., 1999b. Theoretical analysis of hydrophobic matching and membrane-mediated interactions in lipid bilayers containing gramicidin. Biophysical Journal 76, 3176–3185.

Huang, H.W., 1986. Deformation free energy of bilayer membrane and its effect on gramicidin channel lifetime. Biophysical Journal 50, 1061–1070.

Humphrey, W., Dalke, A., Schulten, K., 1996. VMD: visual molecular dynamics. Journal of Molecular Graphics 14, 33–38.

Jardetzky, O., 1966. Simple allosteric model for membrane pumps. Nature 211, 969–970.

Jo, S., Lim, J.B., Klauda, J.B., Im, W., 2009. CHARMM-GUI membrane builder for mixed bilayers and its application to yeast membranes. Biophysical Journal 97, 50–58.

Khelashvili, G., Grossfield, A., Feller, S.E., Pitman, M.C., Weinstein, H., 2009a. Structural and dynamic effects of cholesterol at preferred sites of interaction with rhodopsin identified from microsecond length molecular dynamics simulations. Proteins: Structure, Function, and Bioinformatics 76, 403–417.

Khelashvili, G., Harries, D., Weinstein, H., 2009b. Modeling membrane deformations and lipid demixing upon protein–membrane interaction: the BAR dimer adsorption. Biophysical Journal 97, 1626–1635.

Klauda, J.B., Venable, R.M., Freites, J.A., O'Connor, J.W., Tobias, D.J., Mondragon-Ramirez, C., Vorobyov, I., MacKerell Jr., A.D., Pastor, R.W., 2010. Update of the CHARMM all-atom additive force field for lipids: validation on six lipid types. Journal of Physical Chemistry B 114, 7830–7843.

Krishnamurthy, H., Gouaux, E., 2012. X-ray structures of LeuT in substrate-free outward-open and apo inward-open states. Nature 481, 469–474.

Kucerka, N., Tristram-Nagle, S., Nagle, J.F., 2006. Structure of fully hydrated fluid phase lipid bilayers with monounsaturated chains. Journal of Membrane Biology 208, 193–202.

Lomize, A.L., Pogozheva, I.D., Mosberg, H.I., 2011. Anisotropic solvent model of the lipid bilayer. 2. Energetics of insertion of small molecules, peptides, and proteins in membranes. Journal of Chemical Information and Modeling 51, 930–946.

Lomize, M.A., Lomize, A.L., Pogozheva, I.D., Mosberg, H.I., 2006. OPM: orientations of proteins in membranes database. Bioinformatics 22, 623–625.

Lundbæk, J.A., Andersen, O.S., 1999. Spring constants for channel-induced lipid bilayer deformations estimates using gramicidin channels. Biophysical Journal 76, 889–895.

Lundbaek, J.A., Andersen, O.S., Werge, T., Nielsen, C., 2003. Cholesterol-induced protein sorting: an analysis of energetic feasibility. Biophysical Journal 84, 2080–2089.

Lundbaek, J.A., Birn, P., Tape, S.E., Toombes, G.E.S., Sogaard, R., Koeppe II, R.E., Gruner, S.M., Hansen, A.J., Andersen, O.S., 2005. Capsaicin regulates voltage-dependent sodium channels by altering lipid bilayer elasticity. Molecular Pharmacology 68, 680–689.

Marsh, D., 2007. Lateral pressure profile, spontaneous curvature frustration, and the incorporation and conformation of proteins in membranes. Biophysical Journal 93, 3884–3899.

Marsh, D., 2008. Energetics of hydrophobic matching in lipid–protein interactions. Biophysical Journal 94, 3996–4013.

Mondal, S., Khelashvili, G., Shan, J., Andersen, O.S., Weinstein, H., 2011. Quantitative modeling of membrane deformations by multihelical membrane proteins: application to G-protein coupled receptors. Biophysical Journal 101, 2092–2101.

Mondal, S., Khelashvili, G., Wang, H., Provasi, D., Andersen, O.S., Filizola, M., Weinstein, H., 2012. Interaction with the membrane uncovers essential differences between highly homologous GPCRs. Biophysical Journal 102, 514a.

Moon, C.P., Fleming, K.G., 2011. Side-chain hydrophobicity scale derived from transmembrane protein folding into lipid bilayers. Proceedings of the National Academy of Sciences of the United States of America 108, 10174.

Murzyn, K., Rog, T., Pasenkiewicz-Gierula, M., 2005. Phosphatidylethanolamine–phosphatidylglycerol bilayer as a model of the inner bacterial membrane. Biophysical Journal 88, 1091–1103.

Nielsen, C., Goulian, M., Andersen, O.S., 1998. Energetics of inclusion-induced bilayer deformations. Biophysical Journal 74, 1966–1983.

Nyola, A., Karpowich, N.K., Zhen, J., Marden, J., Reith, M.E., Wang, D.N., 2010. Substrate and drug binding sites in LeuT. Current Opinion in Structural Biology 20, 415–422.

Pantano, D.A., Klein, M.L., 2009. Characterization of membrane protein interactions for the leucine transporter from *Aquifex aeolicus* by molecular dynamics calculations. Journal of Physical Chemistry B 113, 13715–13722.

Perez, C., Koshy, C., Ressl, S., Nicklisch, S., Kramer, R., Ziegler, C., 2011. Substrate specificity and ion coupling in the Na^+/betaine symporter BetP. The EMBO Journal 30, 1221–1229.

Periole, X., Huber, T., Marrink, S.J., Sakmar, T.P., 2007. G protein-coupled receptors self-assemble in dynamics simulations of model bilayers. Journal of the American Chemical Society 129, 10126–10132.

Perozo, E., Kloda, A., Cortes, D.M., Martinac, B., 2002. Physical principles underlying the transduction of bilayer deformation forces during mechanosensitive channel gating. Nature & Structural Molecular Biology 9, 696–703.

Phillips, J.C., Braun, R., Wang, W., Gumbart, J., Tajkhorshid, E., Villa, E., Chipot, C., Skeel, R.D., Kale, L., Schulten, K., 2005. Scalable molecular dynamics with NAMD. Journal of Computational Chemistry 26, 1781–1802.

Phillips, R., Ursell, T., Wiggins, P., Sens, P., 2009. Emerging roles for lipids in shaping membrane–protein function. Nature 459, 379–385.

Piscitelli, C.L., Gouaux, E., 2012. Insights into transport mechanism from LeuT engineered to transport tryptophan. The EMBO Journal 31, 228–235.

Piscitelli, C.L., Krishnamurthy, H., Gouaux, E., 2010. Neurotransmitter/sodium symporter orthologue LeuT has a single high-affinity substrate site. Nature 468, 1129–1132.

Pitman, M.C., Grossfield, A., Suits, F., Feller, S.E., 2005. Role of cholesterol and polyunsaturated chains in lipid–protein interactions: molecular dynamics simulation of rhodopsin in a realistic membrane environment. Journal of the American Chemical Society 127, 4576–4577.

Quick, M., Shi, L., Zehnpfennig, B., Weinstein, H., Javitch, J.A., 2012. Experimental conditions can obscure the second high-affinity site in LeuT. Nature & Structural Molecular Biology 19, 207–211.

Quick, M., Winther, A.M.L., Shi, L., Nissen, P., Weinstein, H., Javitch, J.A., 2009. Binding of an octylglucoside detergent molecule in the second substrate (S2) site of LeuT establishes an inhibitor-bound conformation. Proceedings of the National Academy of Sciences of the United States of America 106, 5563–5568.

Raetz, C.R., 1978. Enzymology, genetics, and regulation of membrane phospholipid synthesis in *Escherichia coli*. Microbiological Reviews 42, 614–659.

Rawicz, W., Olbrich, K.C., McIntosh, T., Needham, D., Evans, E., 2000. Effect of chain length and unsaturation on elasticity of lipid bilayers. Biophysical Journal 79, 328–339.

Rusinova, R., Herold, K.F., Sanford, R.L., Greathouse, D.V., Hemmings Jr., H.C., Andersen, O.S., 2011. Thiazolidinedione insulin sensitizers alter lipid bilayer properties and voltage-dependent sodium channel function: implications for drug discovery. Journal of General Physiology 138, 249–270.

Saier Jr., M.H., 1999. A functional phylogenetic system for the classification of transport proteins. Journal of Cellular Biochemistry 75, 84–94.

Sali, A., Blundell, T.L., 1993. Comparative protein modelling by satisfaction of spatial restraints. Journal of Molecular Biology 234, 779–815.

Sankararamakrishnan, R., Weinstein, H., 2002. Positioning and stabilization of dynorphin peptides in membrane bilayers: the mechanistic role of aromatic and basic residues revealed from comparative MD simulations. Journal of Physics and Chemistry B 106, 209–218.

Shaffer, P.L., Goehring, A., Shankaranarayanan, A., Gouaux, E., 2009. Structure and mechanism of a Na^+-independent amino acid transporter. Science 325, 1010–1014.

Shaikh, S.A., Tajkhorshid, E., 2010. Modeling and dynamics of the inward-facing state of a Na^+/Cl^- dependent neurotransmitter transporter homologue. PLoS Computational Biology 6, e1000905.

Shan, J., Javitch, J.A., Shi, L., Weinstein, H., 2011. The substrate-driven transition to an inward-facing conformation in the functional mechanism of the dopamine transporter. PloS One 6, e16350.

Shan, J., Khelashvili, G., Mondal, S., Mehler, E.L., Weinstein, H., 2012. Ligand-dependent conformations and dynamics of the serotonin $5\text{-}HT_{2A}$ receptor determine its activation and membrane-driven oligomerization properties. PLoS Computational Biology 8, e1002473.

Shi, L., Quick, M., Zhao, Y., Weinstein, H., Javitch, J.A., 2008. The Mechanism of a Neurotransmitter:Sodium Symporter inward release of Na^+ and substrate is triggered by substrate in a second binding site. Molecular Cell 30, 667–677.

Shi, L., Weinstein, H., 2010. Conformational rearrangements to the intracellular open states of the LeuT and ApcT transporters are modulated by common mechanisms. Biophysical Journal 99, L103–L105.

Singh, S.K., Piscitelli, C.L., Yamashita, A., Gouaux, E., 2008. A competitive inhibitor traps LeuT in an open-to-out conformation. Science 322, 1655–1661.

Singh, S.K., Yamashita, A., Gouaux, E., 2007. Antidepressant binding site in a bacterial homologue of neurotransmitter transporters. Nature 448, 952–956.

Sonders, M.S., Quick, M., Javitch, J.A., 2005. How did the neurotransmitter cross the bilayer? A closer view. Current Opinion in Neurobiology 15, 296–304.

Soubias, O., Niu, S.L., Mitchell, D.C., Gawrisch, K., 2008. Lipid-rhodopsin hydrophobic mismatch alters rhodopsin helical content. Journal of the American Chemical Society 130, 12465–12471.

Soubias, O., Teague Jr., W.E., Hines, K.G., Mitchell, D.C., Gawrisch, K., 2010. Contribution of membrane elastic energy to rhodopsin function. Biophysical Journal 99, 817–824.

Strandberg, E., Killian, J.A., 2003. Snorkeling of lysine side chains in transmembrane helices: how easy can it get? FEBS Letters 544, 69–73.

Strandberg, E., Tiltak, D., Ehni, S., Wadhwani, P., Ulrich, A.S., 2012. Lipid shape is a key factor for membrane interactions of amphipathic helical peptides. Biochimica et Biophysica Acta (BBA)—Biomembranes, 1764–1776.

Wang, H., Elferich, J., Gouaux, E., 2012. Structures of LeuT in bicelles define conformation and substrate binding in a membrane-like context. Nature & Structural Molecular Biology 19, 212–219.

Yamashita, A., Singh, S.K., Kawate, T., Jin, Y., Gouaux, E., 2005. Crystal structure of a bacterial homologue of Na^+/Cl^--dependent neurotransmitter transporters. Nature 437, 215–223.

Zhao, C., Stolzenberg, S., Gracia, L., Weinstein, H., Noskov, S., Shi, L., 2012. Ion-controlled conformational dynamics in the outward-open transition from an occluded state of LeuT. Biophysical Journal 103, 878–888.

Zhao, Y., Terry, D., Shi, L., Weinstein, H., Blanchard, S.C., Javitch, J.A., 2010. Single-molecule dynamics of gating in a neurotransmitter transporter homologue. Nature 465, 188–193.

Zhao, Y., Terry, D.S., Shi, L., Quick, M., Weinstein, H., Blanchard, S.C., Javitch, J.A., 2011. Substrate-modulated gating dynamics in a Na^+-coupled neurotransmitter transporter homologue. Nature 474, 109–113.

Zhou, Z., Zhen, J., Karpowich, N.K., Law, C.J., Reith, M.E.A., Wang, D.-N., 2009. Antidepressant specificity of serotonin transporter suggested by three LeuT-SSRI structures. Nature & Structural Molecular Biology 16, 652–657.

Supplementary Material

The cost of living in the membrane: A case study of hydrophobic mismatch for the multi-segment protein LeuT

Sayan Mondal[a], George Khelashvili[a], Lei Shi[a,b], and Harel Weinstein[a,b]

[a] Department of Physiology and Biophysics, [b]The HRH Prince Alwaleed Bin Talal Bin Abdulaziz Alsaud Institute for Computational Biomedicine, Weill Cornell Medical College, Cornell University, New York, NY 10065

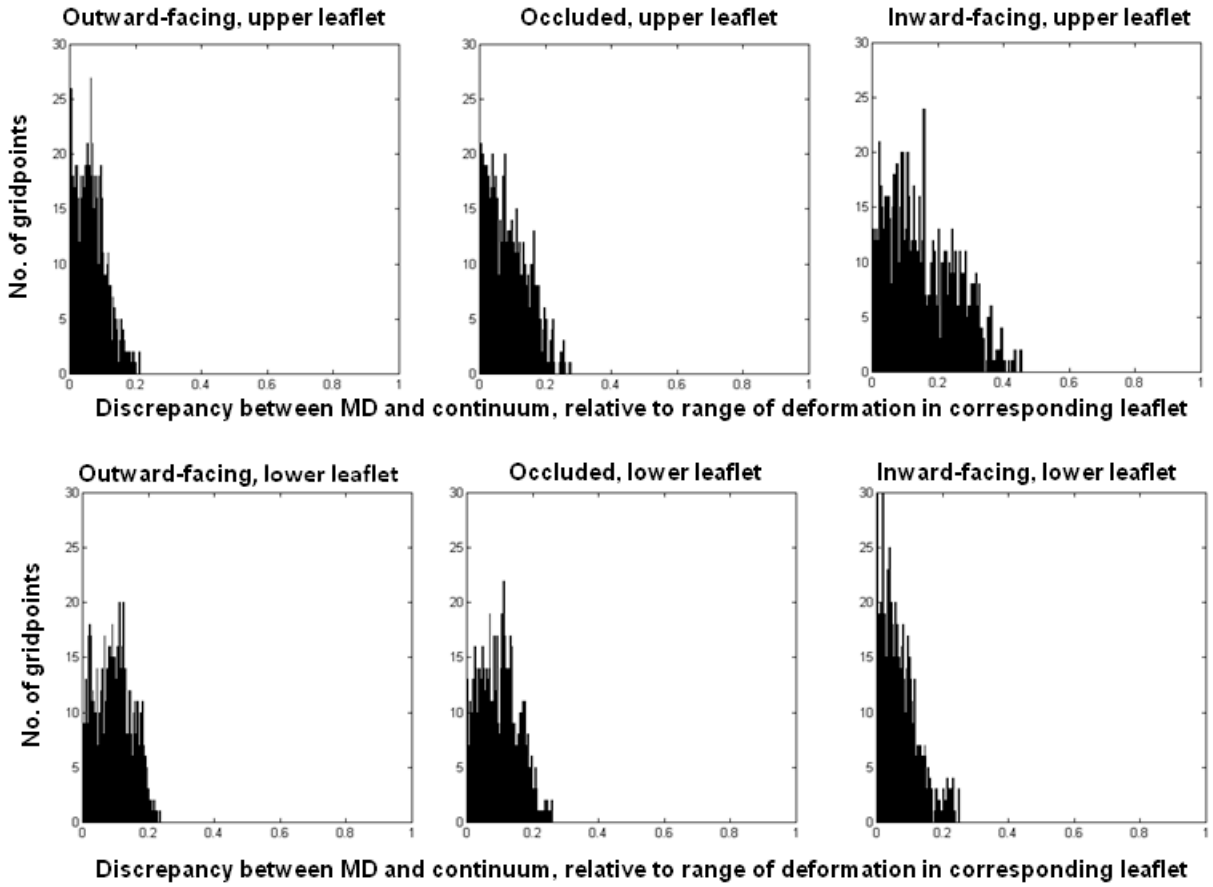

Figure S1 Histograms of the difference between membrane deformations calculated directly from MD, and from continuum-level calculations. Results are shown for the outward-open, occluded, and inward-open conformations of LeuT in POPC. Note that for these calculations, we excluded the gridpoints that were not occupied by lipids due to the embedded protein, as well as the gridpoints on lipid-protein interface where the deformation was taken from MD. As these histograms show, there is a general agreement between calculations at the macroscopic and the microscopic levels, with most gridpoints exhibiting a discrepancy of ~10% of the overall deformation in the corresponding leaflet.

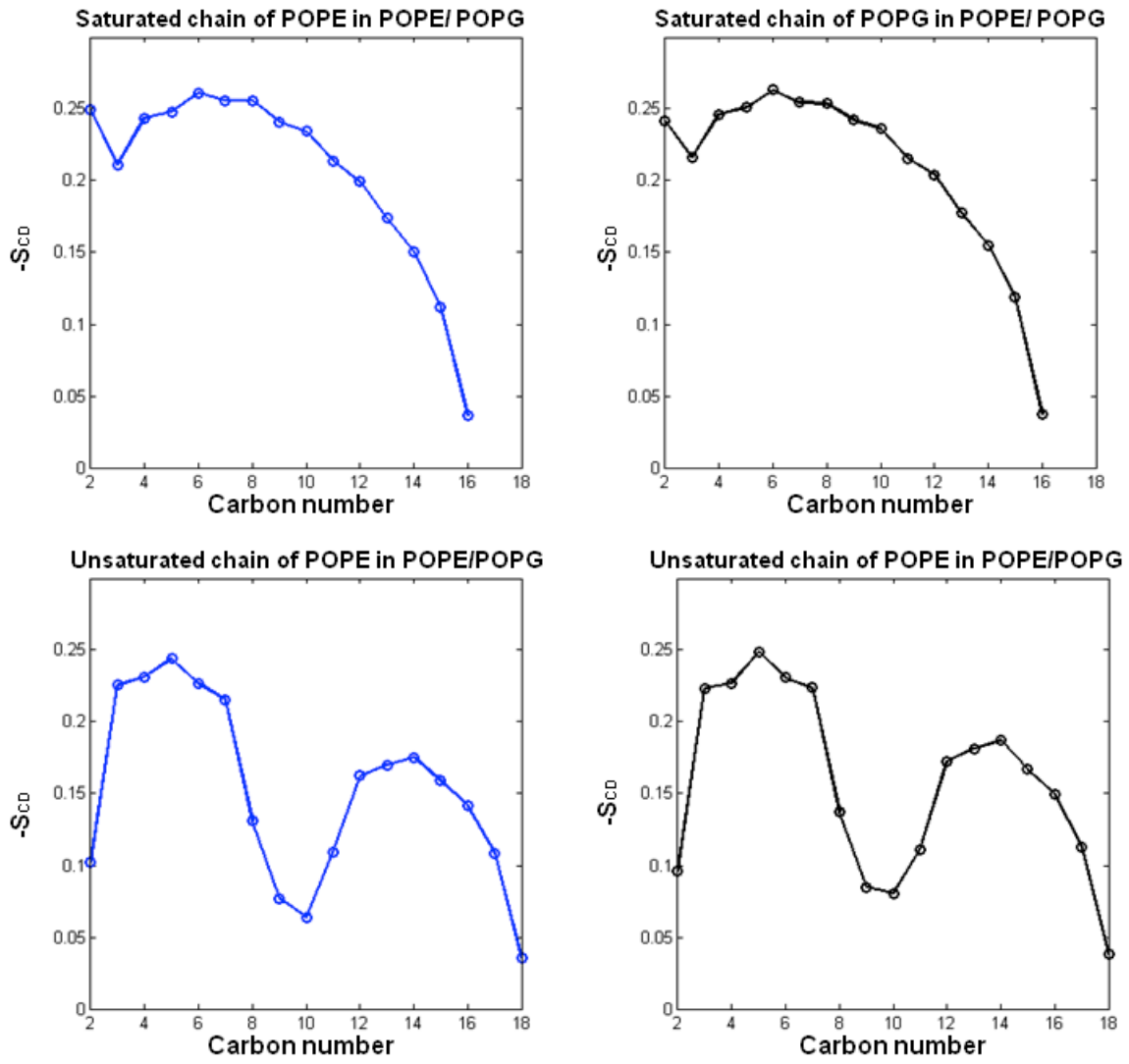

Figure S2 Lipid tail deuterium order parameter ($-S_{CD}$) for POPE (blue) and POPG (black) in the 3:1 mixture of POPE and POPG, calculated for lipids more than 20 Å away from LeuT. These were calculated from the last 12 ns of the MD trajectory for the 3GJD structure with Leu in the S1 site (Table 1 contains a list of molecular constructs used here). The results agree with spectroscopic data for POPE/ POPG lipid mixtures (Salnikov et al., 2009). The order parameters for POPE in the POPE/ POPG lipid mixture here are closer to the values reported for POPE in the liquid crystalline state than in the gel state (Leekumjorn and Sum, 2007), e.g., the maximum of $|S_{CD}|$ is about ~0.25 in both chains for POPE, and decreases to below 0.1 at the 9^{th} and 10^{th} Carbons in the unsaturated chain. The order parameters for POPG in the POPE/ POPG lipid mixture here are similar to what was obtained with the C36 forcefield for POPG in a POPC/ POPG lipid mixture (Janosi and Gorfe, 2010), and only slightly higher in the case of POPE/ POPG. The slightly higher order parameters of POPG in the POPE/POPG mixture are possibly due to the extensive H-bonding in the POPE/ POPG lipid mixture (Murzyn et al., 2005).

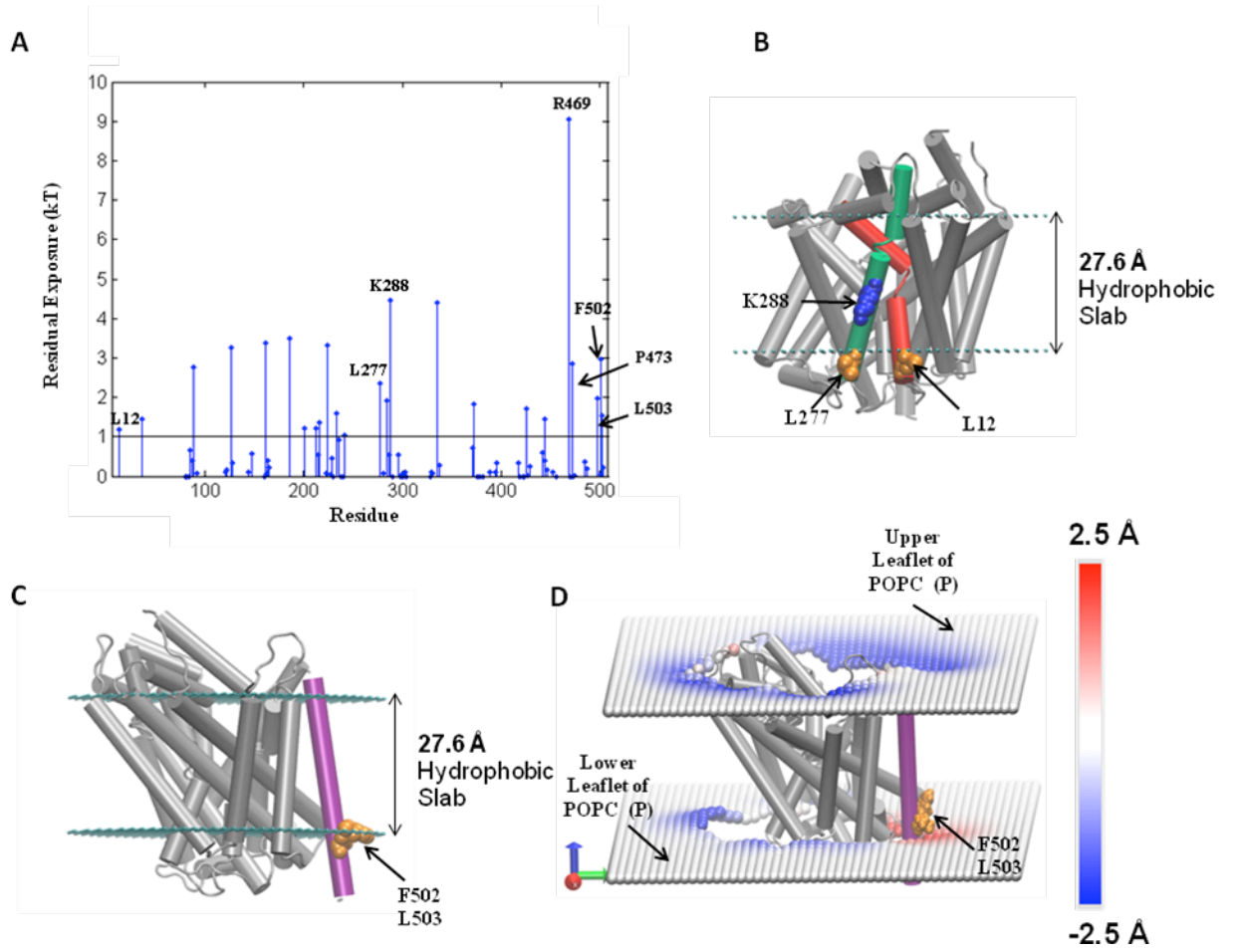

Figure S3 Residual exposure profile for a LeuT monomer positioned in a hydrophobic slab of adjustable thickness. The calculation was done with the Orientations of Proteins in Membranes (OPM) web utility PPM 2.0 (Lomize et al., 2011; Lomize et al., 2006). The LeuT structure for this calculation is from PDBid 3F3A (Singh et al., 2008) for the outward-open, 3GJD (Quick et al., 2009) for the occluded, and 3TT3 (Krishnamurthy and Gouaux, 2012) for the inward-open conformations. The average hydrophobic thickness values calculated for the corresponding structures are 27.6 ± 0.7 Å, 27.0 ± 2.2 Å, and 28.2 ± 1.4 Å, respectively. To calculate the residual exposure in the OPM-positioned protein, solvent accessible surface areas were obtained first with the linear combination of pairwise overlaps approach (Weiser et al., 1999). Only atoms at the membrane-protein interface were considered, with the criteria of <5 Å outside the hydrophobic slab in the Z-direction and <5 Å from the protein-slab boundary in the X-Y plane. The calculations do not consider alleviation of hydrophobic mismatch by snorkeling of Lys and Arg. (**A**) The energy costs for residual exposure of residues to unfavorable hydrophobic-polar interactions, calculated with the CTMDapp http://memprotein.org/resources/servers-and-software. (**B**) Illustrative example of residues where the residual exposure is not alleviated by membrane deformations in POPC from CTMD-based calculations in the main text. The polar residue K288 (in *blue*) is within the hydrophobic milieu, whereas the hydrophobic residues L12

and L277 (*orange*) are outside the hydrophobic milieu. (**C**) Illustrative example of residues where the residual exposure is alleviated by local membrane deformations in POPC (see Fig. 1). The hydrophobic residues that reside partly *outside* the hydrophobic slab are: F502 (in *orange*) and L503 of TM12 (*purple*). (**D**) Local thickening of the cytoplasmic leaflet of POPC (indicated in *red*) occurs near the residues F502 and L503 (*orange*) of TM12 (*purple*).

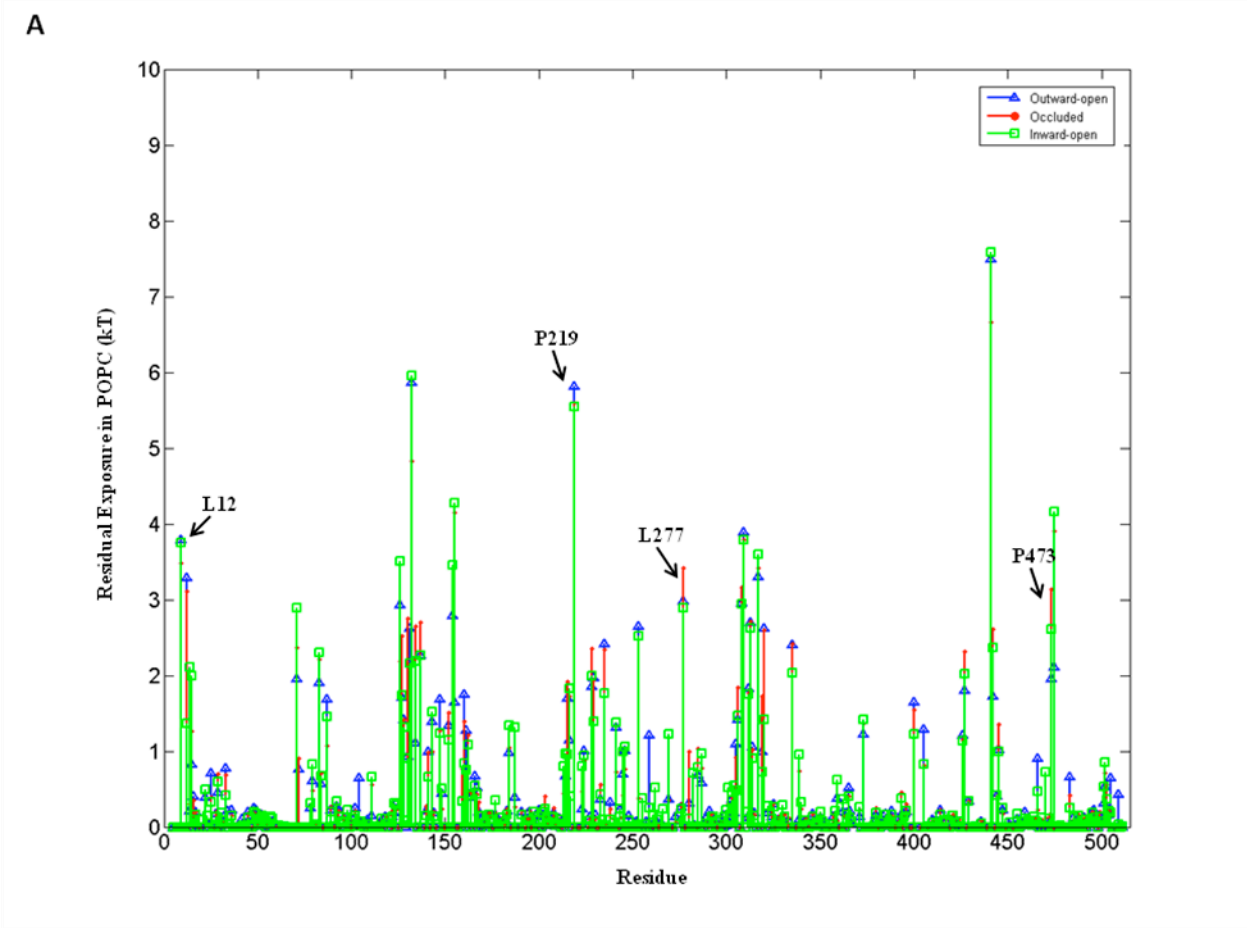

Figure S4 (A) Residual exposure penalties for all residues of LeuT in the outward-open conformation embedded in a POPC lipid bilayer. Note that for certain residues, e.g., F502 and L503 at the intracellular end of TM12, there is no appreciable residual exposure even though these residues were exposed outside OPM-based the hydrophobic slab (Fig. S1). The reason is shown in Fig. S1D where F502 and L503 are seen to be located near the *red* region (thickening) of the cytoplasmic leaflet.

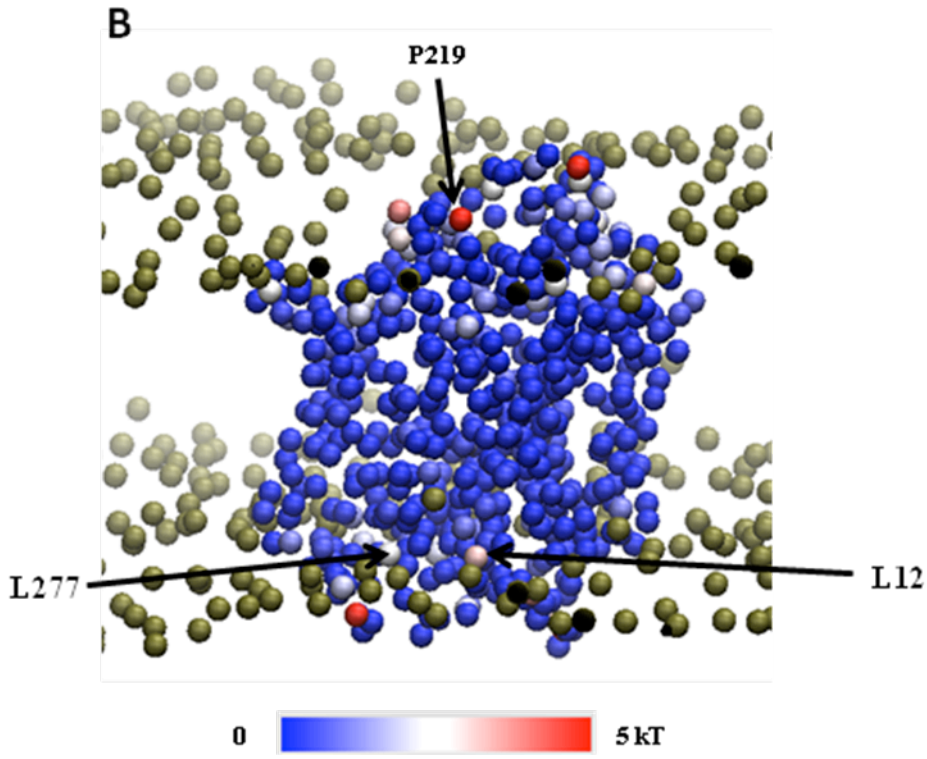

Figure S4 (B) The residual exposure penalties mapped onto the C-*alpha* atoms in the outward-open conformation of LeuT. The surrounding phosphate headgroups are shown (in *tan* coloring) to help identify the membrane-facing residues of the protein. Note that some residues that are not membrane-facing are indicated to have large energy values in Fig. S2A, e.g., at P219, but these are not part of the lipid-protein interactions. On the other hand, residues such as L12 and L277 do face the membrane, and the energy values involve hydrophobic mismatch between the membrane and the protein.

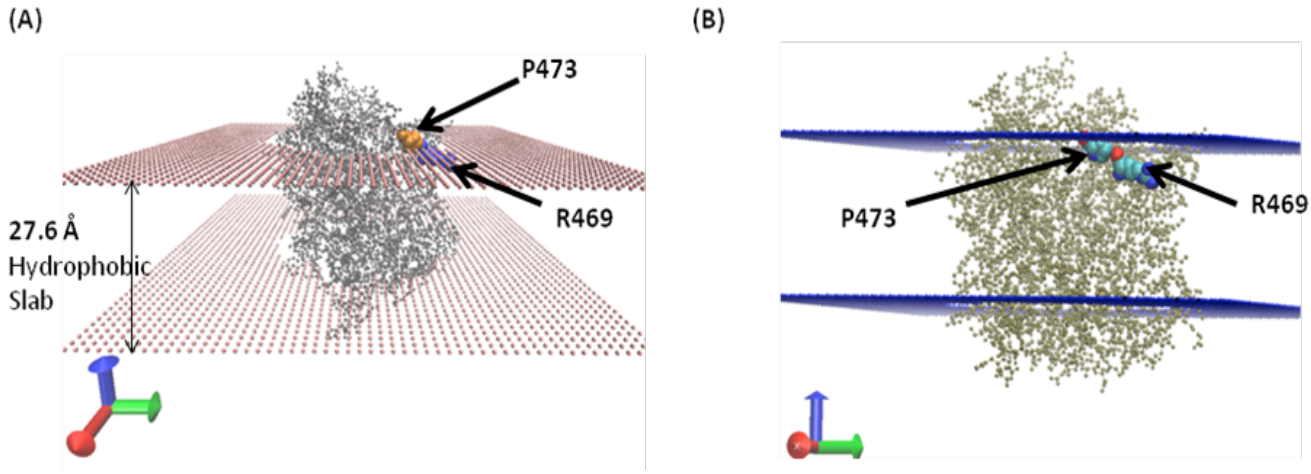

Figure S5 Assessment of the residual exposure at P473 in the X-ray structure of LeuT (PDBid 3F3A) with the OPM-based method (see Fig. S1). **(A)** Exposure of P473 outside the hydrophobic milieu from the OPM-based calculation in Fig. S1. The residual exposure at P473 is 2.8 kT here. **(B)** The thickness of the hydrophobic milieu is extended to 30.8 Å in the Z>0 part corresponding to the upper leaflet. The residual exposure at P473 is reduced to ~0.05 kT. However, in this configuration, R469 is embedded the hydrophobic milieu at > 8.2 Å along just the Z-direction from the position of the P-atoms (assuming a distance of at least 5 Å of P-atoms from the hydrophobic core for POPC (Kucerka et al., 2006)).

References

Janosi, L., Gorfe, A.A., 2010. Simulating POPC and POPC/POPG Bilayers: Conserved Packing and Altered Surface Reactivity. Journal of Chemical Theory and Computation 6, 3267-3273.

Krishnamurthy, H., Gouaux, E., 2012. X-ray structures of LeuT in substrate-free outward-open and apo inward-open states. Nature 481, 469-474.

Kucerka, N., Tristram-Nagle, S., Nagle, J.F., 2006. Structure of fully hydrated fluid phase lipid bilayers with monounsaturated chains. J. Membr. Biol. 208, 193-202.

Leekumjorn, S., Sum, A.K., 2007. Molecular Characterization of Gel and Liquid-Crystalline Structures of Fully Hydrated POPC and POPE Bilayers. J. Phys. Chem. B 111, 6026-6033.

Lomize, A.L., Pogozheva, I.D., Mosberg, H.I., 2011. Anisotropic Solvent Model of the Lipid Bilayer. 2. Energetics of Insertion of Small Molecules, Peptides, and Proteins in Membranes. Journal of Chemical Information and Modeling 51, 930-946.

Lomize, M.A., Lomize, A.L., Pogozheva, I.D., Mosberg, H.I., 2006. OPM: orientations of proteins in membranes database. Bioinformatics 22, 623-625.

Murzyn, K., Rog, T., Pasenkiewicz-Gierula, M., 2005. Phosphatidylethanolamine-phosphatidylglycerol bilayer as a model of the inner bacterial membrane. Biophys. J. 88, 1091-1103.

Quick, M., Winther, A.M.L., Shi, L., Nissen, P., Weinstein, H., Javitch, J.A., 2009. Binding of an octylglucoside detergent molecule in the second substrate (S2) site of LeuT establishes an inhibitor-bound conformation. Proc. Natl. Acad. Sci. USA 106, 5563-5568.

Salnikov, E.S., Mason, A.J., Bechinger, B., 2009. Membrane order perturbation in the presence of antimicrobial peptides by 2H solid-state NMR spectroscopy. Biochimie 91, 734-743.

Singh, S.K., Piscitelli, C.L., Yamashita, A., Gouaux, E., 2008. A competitive inhibitor traps LeuT in an open-to-out conformation. Science 322, 1655-1661.

Weiser, J., Shenkin, P.S., Still, W.C., 1999. Approximate atomic surfaces from linear combinations of pairwise overlaps (LCPO). Journal of Computational Chemistry 20, 217-230.